[American Journal of Science, Vol. 317, October, 2017, P. 901–940, DOI 10.2475/08.2017.02]

THE LATE NEOPROTEROZOIC DAHANIB MAFIC-ULTRAMAFIC INTRUSION, SOUTH EASTERN DESERT, EGYPT: IS IT AN ALASKAN-TYPE OR A LAYERED INTRUSION?

MOKHLES K. AZER*, HISHAM A. GAHLAN**,***, PAUL D. ASIMOW[§,†], and KHALED M. AL-KAHTANY**

ABSTRACT. In Egypt, mafic-ultramafic complexes have been classified into three major types: incomplete ophiolite sequences; Alaskan-type intrusions, concentrically-zoned bodies formed in a subduction arc environment; and layered intrusions, vertically-zoned bodies intruded in post-collisional tectonic environments and rift-related bodies associated with the opening of the Red Sea. We present new field work, geochemical data, mineral chemistry and interpretations for the late Neoproterozoic Dahanib mafic-ultramafic intrusion in the South Eastern Desert of Egypt (northern-most Arabian–Nubian Shield, ANS). The Dahanib intrusion shows no evidence of metamorphism or deformation, with excellent preservation of intrusive contacts, well-preserved textures and primary mineralogy. Field relations indicate that it is younger than the surrounding metamorphic rocks and syn-tectonic granitoids. The intrusion is composed of a basal suite of ultramafic rocks (dunite, lherzolite, wehrlite and pyroxenite) and an overlying suite of mafic rocks (olivine gabbronorite, gabbronorite and anorthosite). It displays evident layering of modal abundance, visible directly in outcrop, as well as cryptic layering discernible through changes in mineral compositions. The western and eastern lobes of the Dahanib intrusion occur in the form of a lopolith with readily correlated layers, especially in the upper mafic unit. The present-day dip of the layering decreases from the ultramafic units into the mafic sequence. Structural and compositional relations show that the ultramafic units are cumulates from a high-Mg tholeiitic parent magma emplaced at deep crustal levels and evolved via fractional crystallization rather than any kind of residual mantle sequence. Fo content of olivine and Mg# of pyroxenes display a systematic decrease from ultramafic to mafic rocks, well-correlated with whole-rock Mg#. Spinels in ultramafic samples vary from Cr-rich to Al-rich and have Mg# and Fe^{3+}# similar to spinels from typical stratiform complexes and clearly different from those found in ophiolitic and Alaskan-type complexes. Although the mafic and ultramafic units are clearly related and can be derived from common parent magma, they were not emplaced coevally; rather, they represent different pulses of magma. The Dahanib mafic–ultramafic intrusion does not display any features that convincingly identify it as a typical Alaskan-type body, particularly the lack of clinopyroxenite and hornblendite, rarity of primary hornblende, and the notable abundance of orthopyroxene and plagioclase in its rocks. Our results confirm that it is more akin to a layered mafic-ultramafic intrusion with a multistage evolution. It was emplaced into a stable post-orogenic cratonic setting, with a trace element signature indicating contamination of the mantle source by previous subduction events.

Key words: Neoproterozoic, Arabian-Nubian Shield, Eastern Desert, layered intrusion, post-collision

INTRODUCTION

Mafic-ultramafic rocks often provide essential evidence for understanding the geodynamic evolution of orogenic belts. In the Arabian-Nubian Shield (ANS),

* Geological Sciences Department, National Research Centre, 12622-Dokki, Cairo, Egypt
** Department of Geology and Geophysics, King Saud University, Riyadh 11451, Saudi Arabia
*** Geology Department, Assiut University, Assiut 71516, Egypt
§ Division of Geological & Planetary Sciences, California Institute of Technology, Pasadena, California, 91125 USA
† Corresponding author: asimow@gps.caltech.edu

Neoproterozoic mafic-ultramafic complexes are widespread and distinctive members of several tectono-stratigraphic units and have helped to define the nature of those units. At the scale of the whole shield, there are intrusions that relate to ophiolites, to island arcs, to late- or post-collisional activity, and to within-plate rift development. In Egypt in particular, the ages and tectonomagmatic affinities of Precambrian mafic-ultramafic rocks have been classified into older and younger mafic-ultramafic complexes. The older mafic-ultramafic complexes form either an integral part of obducted ophiolite sequences (El Sharkawy and El Bayoumi, 1979; Ali and others, 2010; Gahlan and others, 2015; Obeid and others, 2016) or are members of subduction-related calc-alkaline complexes (for example Farahat and Helmy, 2006; Helmy and others, 2014, 2015; Khedr and Arai, 2016). The younger complexes are mostly fresh, undeformed and unmetamorphosed and are considered to be post-orogenic rocks (Azer and El-Gharbawy, 2011; Abdel Halim and others, 2016) or rift-related intrusions (Bonatti and others, 1986; Brueckner and others, 1995; Bosch and Bruguier, 1998).

A number of such mafic-ultramafic intrusions of Late Neoproterozoic age occur in the South Eastern Desert of Egypt (fig. 1A), namely the Abu Hamamid, Gabbro Akarem, Genina Gharbia, Dahanib, El-Motaghairat and Abu Fas intrusions. These mafic-ultramafic intrusions have been studied by many authors (for example Dixon, 1981a; Hafez and others, 1991; Sadek and El-Ramly, 1996; Helmy and El Mahallawi, 2003; Farahat and Helmy, 2006; Helmy and others, 2008, 2014, 2015; Khedr and Arai, 2016; Abdel Halim and others, 2016), yet there are many issues that are poorly constrained with specific reference to their petrogenesis and tectonic setting. In particular, some authors have concluded that most of them are Alaskan-type intrusions (Helmy and El Mahallawi, 2003; Farahat and Helmy, 2006; Helmy and others, 2008, 2014; Helmy and others, 2015; Khedr and Arai, 2016) while others conclude that they are layered intrusions (Dixon, 1981a; Sadek and El-Ramly, 1996; Abdel Halim and others, 2016).

The term "Alaskan-type intrusion" was first used by Irvine (1974) for mafic–ultramafic intrusions characterized by concentrically-zoned structure starting with dunite in the center and grading outward into wehrlite, olivine clinopyroxenite, clinopyroxenite, hornblende clinopyroxenite, hornblendite and gabbro. The Alaskan-type complexes are considered to be characteristic of island arc magmatism and associated Pt-group element mineralization (for example Irvine, 1974; Johan, 2002; Ishiwatari and Ichiyama, 2004; Pettigrew and Hattori, 2006; Thakurta and others, 2008; Ripley, 2009). It has been noted in the literature that differentiating between Alaskan-type and layered intrusions on the basis of geochemistry alone is difficult (for example Wager and Brown, 1968; Himmelberg and Loney, 1995; Helmy and El Mahallawi, 2003; Ishiwatari and Ichiyama, 2004; Azer and El-Gharbawy, 2011; Charlier and others, 2015; Habtoor and others, 2016). The best way to differentiate between them is field and petrographic studies, at least in those cases where primary structural relations are preserved and exposure is adequate. Paradoxically, despite the difficulty in some cases of distinguishing between Alaskan-type and layered intrusions, the distinction is critical to proper interpretation of the meaning of a mafic-ultramafic intrusion within its regional geologic context. If assigned to Alaskan-type, the intrusion becomes part of a tectonic model requiring active subduction in an island-arc setting. On the other hand, if assigned to layered type, then the intrusion carries no such implication and can plausibly occur in a post-collisional environment without implying a contradiction.

The present work will deal with the Dahanib intrusion, one of the best-preserved mafic-ultramafic intrusions in the ANS, with primary mineralogy and igneous structures. Previous work focused specifically on this body has created much controversy about its origin (El-Ramly, 1972; Dixon, 1981a; El-Gaby and others, 1990; Meguid and El-Metwally, 1998; Khedr and Arai, 2016), due in large part to the lack of detailed field

studies and the paucity of petrological data. El-Ramly (1972) simply grouped the Dahanib intrusion as one of a series of intrusive gabbroic bodies. Dixon (1981a) described it as a layered intrusion associated with an early island arc phase (>710 Ma), fractionated from komatiitic melts. However, Church (1983) doubted that komatiitic rocks could be quantitatively important in the Eastern Desert. On the other hand, some authors described the Dahanib intrusion as late- to post-tectonic (El-Gaby and others, 1990; Geologic Survey of Egypt, 1992; Meguid and El-Metwally, 1998). The earlier interpretation that this complex represents a layered intrusion (Dixon, 1981a) has been refuted in recent studies that classify it instead as an Alaskan-type intrusion (Khedr and Arai, 2016). The Alaskan-type character of the Dahanib intrusion was inferred from mineral chemistry of silicates and limited whole rock chemistry (6 samples) without any field evidence to confirm concentric structure (Khedr and Arai, 2016), despite agreement in the literature that the best way to differentiate between Alaskan-type and layered intrusions is field study, more than geochemistry.

The aim of this paper is to decipher the petrogenesis and tectonic setting of the Dahanib intrusion based on new field work, geochemical data, mineral chemistry and interpretations. As the principal goal is to clarify the issue of Alaskan versus layered character, we present systematic sampling to show both the horizontal extension of the basal peridotites and the vertical layering upwards from basal peridotite through pyroxenite to gabbros. We present structural attitude data, where available, and clear field photographs to support inferred field relations. We also examine whether the mafic and ultramafic rocks of the Dahanib intrusion represent a continuous sequence of cumulates or whether instead there is a break between them. Finally, we place Dahanib in the context of mafic-ultramafic magmatism in the South Eastern Desert and discuss the insights it provides into the magmatic evolution of continental crust in the ANS during Neoproterozoic time.

GEOLOGIC BACKGROUND

General Geology

The Egyptian Eastern Desert and Sinai comprise the northernmost basement outcrops of the ANS (fig. 1A). The ANS is a juvenile crustal tract formed by protracted accretion of oceanic and island arc terranes (~700 Ma), followed by late Neoproterozoic continental collision (~640–650 Ma) and a post-collisional (~640–580 Ma) stage (for example Meert, 2003; Stoeser and Frost, 2006, Be'eri-Shlevin and others, 2011). Finally, the ANS was stabilized by ~530 Ma as a stable craton and platform setting (Garfunkel, 1999; Genna and others, 2002).

Mafic-ultramafic complexes represent important rock units in the Precambrian basement of Egypt. They were formed in various tectonic settings from oceanic to continental margin and continental interior settings. They are distinguished into four main groups: ophiolitic rocks, island-arc intrusions, post-collisional layered intrusions and rift-related intrusions. In ophiolite exposures, mafic-ultramafic complexes are highly metamorphosed, and ultramafic units occupy the basal part of the sequence.

The island-arc mafic-ultramafic rocks are less common in the Eastern Desert of Egypt; the largest one is the Abu Fas intrusion in the South Eastern Desert (Sadek and El-Ramly, 1996). They are slightly metamorphosed and the ultramafic members are partly serpentinized. Recently, some authors (for example Helmy and El Mahallawi, 2003; Farahat and Helmy, 2006; Abd El-Rahman and others, 2012; Helmy and others, 2014, 2015; Khedr and Arai, 2016) applied the term Alaskan-type intrusion to some mafic-ultramafic intrusions in the South Eastern Desert (for example Akarem, Genina Gharbia, Abu Hamamid and Dahanib). They considered these intrusions to be concentrically zoned and to represent the roots of island arcs. However, the zoning is discontinuous and difficult to reconstruct geometrically and the ultramafic members

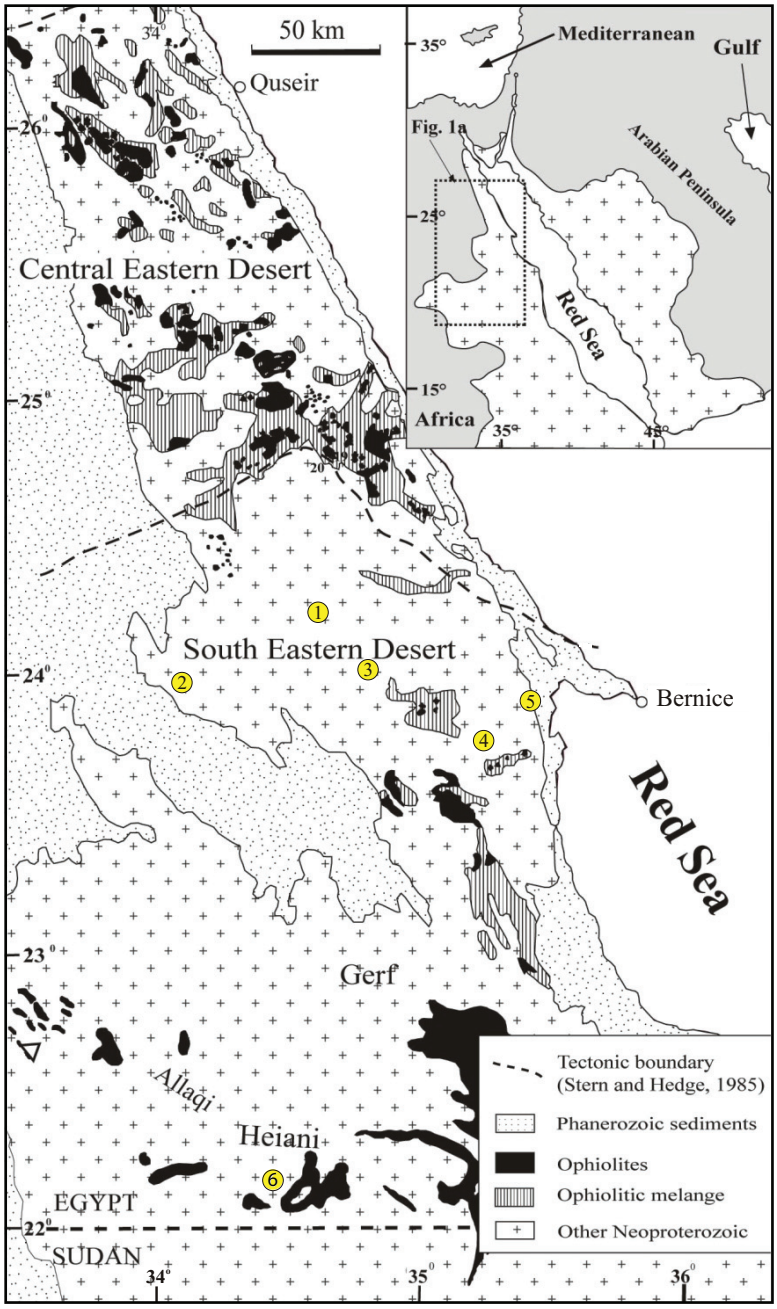

Fig. 1. (A) Regional geologic map of Late Neoproterozoic rocks in the Eastern Desert of Egypt (modified after Shackleton, 1994); inset shows the location of the Eastern Desert relative to the exposure area of the Neoproterozoic Arabian-Nubian Shield of Eastern Africa and Western Arabia. Major late Neoproterozoic mafic-ultramafic intrusions in South Eastern Desert are indicated: (1) Abu Hamamid, (2) Gabbro Akarem, (3) Genina Gharbia, (4) Dahanib, (5) El-Motaghairat, (6) Abu Fas intrusions.

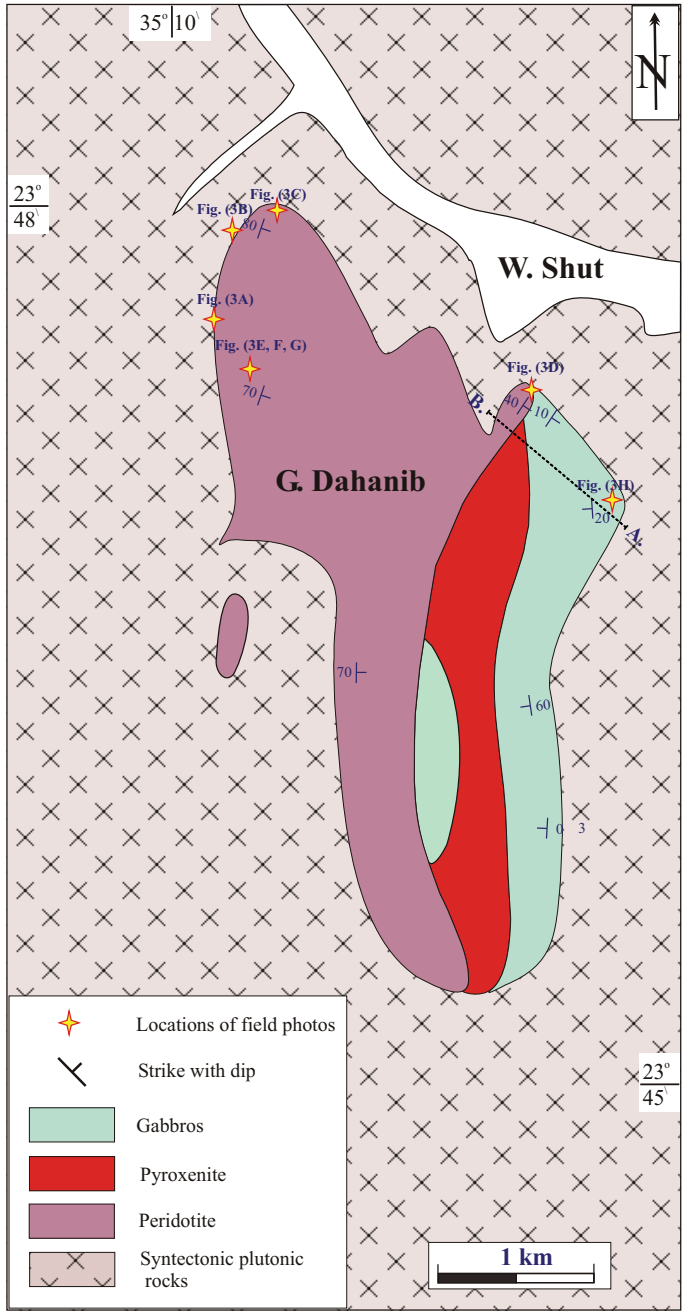

Fig. 1 (continued). (B) Detailed geologic map of the Dahanib intrusion (after Dixon, 1981a). The locations of cross-section of figure (2) and the field photos of figure 3 are indicated.

may be large enclaves within or younger intrusions into the mafic rocks. Also, previous studies revealed that all the so-called Alaskan-type intrusions are fresh and unmetamorphosed (for example Helmy and El Mahallawi, 2003; Farahat and Helmy, 2006; Abd

El-Rahman and others, 2012; Helmy and others, 2014, 2015; Khedr and Arai, 2016). This appears inconsistent with the character of the island-arc phase in the Eastern Desert, which ended before the last collisional event at ~650 Ma and is preserved only in rocks that are largely deformed and metamorphosed, typically to greenschist facies (for example Bentor, 1985; Abdel-Rahman and Doig, 1987; El-Gabby and others, 1990; Mohamed and Hassanen, 1996; Abu El-Ela, 1997).

Post-collisional layered intrusions are very rare in the Precambrian basement of Egypt. A few layered mafic-ultramafic intrusions have been recognized in the South Eastern Desert of Egypt (for example Motaghairat: Ahmed, 1991; Abdel Halim and others, 2016) and in southern Sinai (for example Gabal Imleih: Azer and El-Gharbawy, 2011). These layered mafic-ultramafic intrusions are vertically zoned from ultramafic units at the base upwards into mafic units towards the top of the intrusion. They represent post-collisional intrusions (Azer and El-Gharbawy, 2011; Abdel Halim and others, 2016) and escaped the penetrative deformation and metamorphism associated with the collisional stage.

Rift-related ultramafic units in the Eastern Desert of Egypt are restricted to Zabargad Island, where they may be associated with the opening of the Red Sea (Bonatti and others, 1986; Brueckner and others, 1995; Bosch and Bruguier, 1998). The origin of Zabargad Island is a matter of debate and the ultramafic rocks there may be the result of mantle diapirism during the early rifting of the Red Sea (Boudier and others, 1988).

Geological Setting

The Dahanib complex is located in the South Eastern Desert of Egypt to the southwest of Bernice (fig. 1A). It lies between latitudes 23° 45' and 23° 48' N and longitudes 35° 10' and 35° 11' E. The area shows moderate relief, except for the Gebel (G.) Dahanib (~1270 m above sea level), the highest among several peaks in the area (fig. 1B). Wadi Shut is the major valley (NW–SE) that drains the area around G. Dahanib. The main map-scale units in the area are syntectonic felsic-mafic plutonic rocks and mafic-ultramafic rocks (fig. 1B). The syntectonic mafic-felsic plutonic rocks are deformed and include granodiorite, tonalite, diorite and gabbro. The mafic-ultramafic rocks that are the focus of this study are intruded into the syntectonic plutonic suite. They are common at G. Dahanib with several scattered outcrops to the west of Wadi Shut. Hitherto, geochronological data from the study area are scarce. The syntectonic rocks represent the oldest unit in the area, and one dated quartz diorite yielded a concordant U-Pb zircon age of 710 Ma (Dixon, 1981b). Khedr and Arai (2016) considered this syntectonic, deformed quartz-diorite to be younger than the Dahanib intrusion, but the field observations indicate that the Dahanib intrusion is neither deformed nor metamorphosed.

The intrusion of G. Dahanib (hereafter, the Dahanib intrusion) is a mafic-ultramafic lopolith-like layered intrusion. The cross-section from east to west shows that the western and eastern lobes of the Dahanib intrusion occur in the form of a lopolith, especially the upper unit (fig. 2). The field studies support the existence of matching layers of gabbroic rocks in the western and eastern lobes. The Dahanib intrusion covers ~14 km^2 and forms an elliptical shape trending N-S. It shows well-developed intrusive contacts against the tonalite/granodiorite and gabbro/diorite gneissic country rocks (fig. 3A). Offshoots and apophyses of peridotite (up to a few meters in length) extend from the Dahanib intrusion into the country rocks (fig. 3B). On the other hand, xenoliths of the country rocks (granodiorite) are observed within the northern margins of the intrusion (fig. 3C). A chilled marginal facies, although quite rarely observed, can be identified at the northern and northwestern margins; Dixon (1981a) wrote that he did not find a chilled margin.

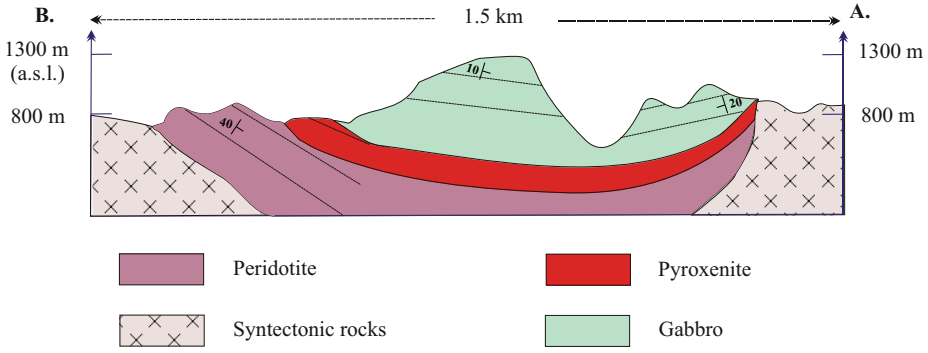

Fig. 2. Generalized northwest-southeast cross section showing the field relationships between the mafic and ultramafic units of the Dahanib intrusion and its country rocks.

Well-developed compositional layering is easily observed throughout the intrusion, especially in the northeastern part (fig. 3D). At map-scale, three major cumulate layers can be identified: the western, structurally lowest cumulate peridotites; the central pyroxenites; and the eastern and structurally highest layered gabbros. The contacts between layers are commonly sharp. Layering in the basal cumulate peridotite mass near the western margin dips from vertical to steeply down to the east (average dip direction/amount = 90/70°) (fig. 3E). The peridotite layer is dominated by cumulate dunite at the base, grading upward into cumulate wehrlite and lherzolite. The cumulate dunite is characterized by massive nature, spheroidal/boulder weathering and deep pink color (fig. 3F). Chromitite layers (~1–5 cm thick) and seams are enveloped by dunite (fig. 3G).

The pyroxenite layer represents almost 25 percent of the total volume of the intrusion. It has sharp boundaries against the basal peridotites and the top gabbros, with no chilled margins. The dominant field texture of the pyroxenites is massive. There are also a few concordant veins of pyroxenite in the peridotite and dunite layers (fig. 3E).

The layered gabbro unit occupies the eastern margin of the outcrop area. It shows sharp intrusive contacts against the tonalite/granodiorite country rocks. In a few outcrops, the contacts between the Dahanib gabbro and the old country rocks are characterized by the presence of hybrid zone. Dixon (1981a) considered this hybrid zone to be a gradational contact from Dahanib gabbro to the granodiorite. The contact against the pyroxenite layer is sharp and is marked by a fine-grained gabbro facies (possible chilled margin). At the eastern limit of the intrusion, layering in the gabbro unit dips 30 to 60° to the west (average dip direction/amount = 275/40°), while structurally and topographically at the top of the intrusion layering is nearly horizontal or slightly inwardly dipping (fig. 3H). A variety of gabbros can be identified within the layer, sometimes with gradational contacts, including gabbro, pegmatitic gabbro and rarely anorthosite. A major gabbro layer is observed in the central zone of the Dahanib intrusion, in direct contact with the basal peridotite layer (fig. 1B).

PETROGRAPHY

Modal abundances of minerals from point counting of thin sections representing each lithology are presented in table 1. The details of petrographic observations for the observed rock types are summarized below.

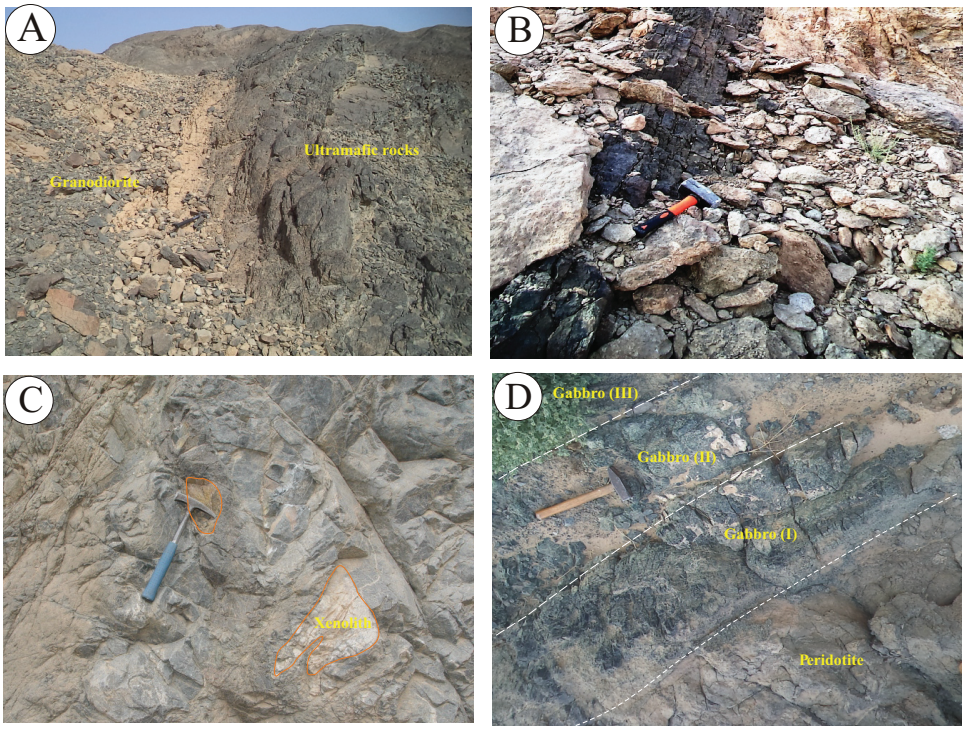

Fig. 3. Field photos of the Dahanib intrusion. (A) Intrusive contact between the ultramafic rocks of the Dahanib intrusion and the granodiorite, (B) offshoot of peridotite extending from the Dahanib intrusion into the country rocks, (C) xenoliths of the country rocks (granodiorite) within the northern margin of the Dahanib intrusion, (D) well-developed compositional layering in the Dahanib intrusion; the modal olivine decreases from gabbro (I) to gabbro (III).

Ultramafic Rocks

The ultramafic rocks (forming the lower part of the layered intrusion) include dunite, wehrlite, lherzolite and pyroxenite. They are commonly coarse-grained and unmetamorphosed.

Dunite is dominated by olivine (90–95%) with minor clinopyroxene and orthopyroxene, if any (fig. 4A). It shows a well-developed adcumulate texture. Spinel and magnetite are the common accessories. It is occasionally chrome-rich (contains > 3% chromian spinel). Olivine forms Y-cracked subhedral crystals, with a weak magmatic preferred orientation. Pyroxenes form subhedral interstitial crystals. Spinel forms disseminated reddish brown homogenous euhedral to subhedral crystals, and is sometimes included in olivine. Magnetite forms euhedral to subhedral crystals commonly disseminated throughout the rock.

Wehrlite consists mainly of olivine and clinopyroxene (fig. 4B). It shows either orthocumulate or poikilitic texture. Interstitial traces of orthopyroxene and plagioclase are not uncommon. Spinel and magnetite are the common accessories. Olivine (45–60%) forms subhedral to anhedral cumulus crystals, as well as chadacrysts included in clinopyroxene. Clinopyroxene (35–55%), mainly diopside, forms large subhedral (oikocryst) to anhedral (intercumulus) crystals. Spinel shows a yellowish-brown color and euhedral to subhedral forms. Euhedral magnetite crystals are largely disseminated throughout the rock.

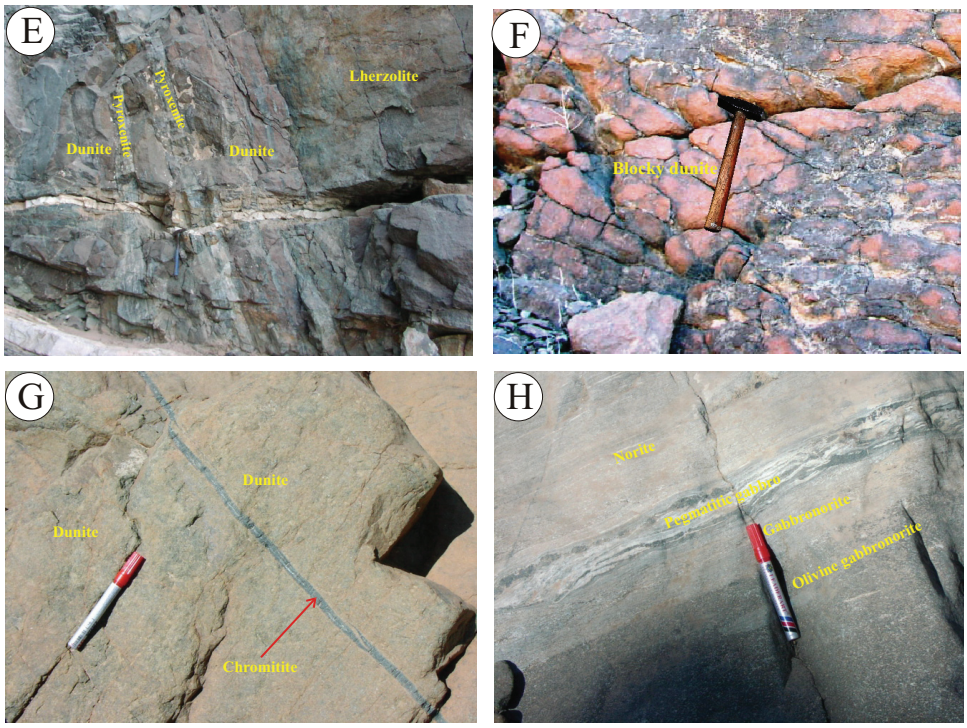

Fig. 3 (continued). (E) Nearly vertical layering in the basal ultramafic rocks where the pyroxenite veins cut the dunite, (F) massive cumulate dunite with deep pink color, (G) chromitite layer enveloped by dunite, and (H) layering in the gabbro unit starting with olivine gabbronorite at the base through gabbronorite to anorthosite at the top of the intrusion.

Lherzolite consists mainly of olivine (~55–70%), and variable proportions of clinopyroxene and orthopyroxene, with minor plagioclase. It shows a well-developed orthocumulate texture with triple points between the constituent minerals, as well as a conspicuous preferred orientation. Yellowish-brown or green spinels and magnetite are the common accessories. Olivine forms subhedral to anhedral crystals and occasionally chadacrysts included in clinopyroxene. Pyroxenes form interstitial/intercumulus phases, as well as oikocrysts. Clinopyroxene (diopside) is found as subhedral crystals as well as exsolution lamellae in orthopyroxene. Orthopyroxene (enstatite) oikocrysts sometimes include clinopyroxene chadacrysts. Plagioclase forms anhedral intercumulus crystals intergrown with clinopyroxene (fig. 4C). Spinel and magnetite form euhedral to subhedral crystals, disseminated or included in silicate phases. The green spinel (pleonaste) is concentrated in clusters of subhedral grains or rounded crystals (fig. 4D).

Pyroxenites include olivine websterite and websterite (figs. 4E and 4F). Both types consist mainly of clinopyroxene and orthopyroxene as cumulus mineral phases. Plagioclase is observed as a minor constituent in olivine websterite. Hornblende is only recorded in websterite as an accessory mineral. Magnetite is the common accessory mineral in both olivine websterite and websterite. The pyroxenites show mesocumulate to adcumulate textures, occasionally with a well-developed preferred orientation. Triple points between mineral phases can be easily observed. Clinopyroxene (diopside) is commonly coarser than orthopyroxene (enstatite), and there are some oikocrysts of diopside including chadacrysts of enstatite.

Table 1

Modal mineralogy of each rock type in the Dahanib intrusion from point counting of petrographic thin sections

Rock type	Dunite		Lherzolite		Wehrlite		Pyroxenites				Gabbros					
							Olivine websterite	Websterite	Olivine gabbronorite		Gabbronorite		Norite		Anorthosite	Fine-grained gabbro
Sample number	DH7	DH10	DH15	DH26	DH13	DH45	DH40	DH42	DH44	DH46	DH21	DH48	DH22	DH25	DH58	DH50
Olivine	89.6	94.7	55.3	69.9	44.5	60.4	6.6	-	5.8	6.1	-	0.5	-	-	-	-
Plagioclase	-	-	0.3	0.4	0.1	0.8	1.4	-	64.5	49.6	54.1	53.2	39.9	64.5	92.7	62.8
Orthopyroxene	0.5	0.1	19.3	12.5	0.3	0.6	42.3	45.3	19.4	30.4	32.4	31.2	35.4	24.7	1.8	4.6
Clinopyroxene	2.3	0.6	19.5	13.2	54.5	35.4	46.8	51.2	6.4	9.2	7.6	8.6	9.6	3.7	1.6	23.8
Amphibole	-	-	-	-	-	-	-	1.3	1.4	1.1	1.7	2.5	7.8	4.2	0.9	-
Opaques	1.5	0.4	2.1	1.6	0.2	0.9	1.8	1.5	1.7	2.2	3.1	2.7	4.7	2.1	1.3	6.7
Cr-spinel	3.2	3.1	1.1	0.5	0.2	0.7	-	-	-	-	-	-	-	-	-	-
Accessory and secondary minerals	2.9	1.1	2.4	1.9	0.2	1.4	1.1	0.7	0.8	1.4	1.1	1.3	2.6	1.1	1.7	2.1

Mafic Rocks

The mafic rocks (forming the upper layer of the intrusion) include olivine gabbronorite, gabbronorite, norite and anorthosite. Except for the fine-grained gabbro at the pyroxenite contact, the Dahanib gabbros are commonly medium to coarse-grained and occasionally layered.

Olivine gabbronorite shows a hypidiomorphic granular texture (fig. 4G). Occasionally, it exhibits a magmatic preferred orientation. It consists mainly of plagioclase (50–65%), clinopyroxene and orthopyroxene, with subordinate amounts of olivine and minor amphiboles. The accessory minerals include magnetite, ilmenite and rare apatite. Plagioclase (An_{70-82}) forms subhedral tabular crystals and displays polysynthetic twining. Clinopyroxene (diopside) and orthopyroxene (hypersthene) form subhedral crystals and are rimmed by secondary amphiboles. Olivine forms anhedral to subhedral separated crystals or is included in pyroxene. Magnetite and ilmenite are largely disseminated throughout the rock, or sometimes form striations along cleavage planes of pyroxenes.

Gabbronorite is largely similar to olivine gabbronorite (fig. 4H), except for the absence of olivine. Plagioclase anorthite content ranges from 40 to 70. It shows characteristic anti-ophitic and ophitic textures. The modal abundance of orthopyroxene exceeds that of clinopyroxene (diopside).

Norite consists mainly of plagioclase (40–65%) and orthopyroxene (25–35%), with minor hornblende. Magnetite, ilmenite, zircon and apatite are the common accessories. It shows orthocumulate texture, as well as a magmatic preferred orientation. Plagioclase forms zoned subhedral crystals, with a characteristic polysynthetic twining. It represents the cumulus phase. Orthopyroxene (enstatite) forms subhedral interstitial crystals. Hornblende forms subhedral to anhedral fine interstitial crystals among the other constituents, with a conspicuous brownish green color. Ilmenite and magnetite form anhedral disseminated crystals, as well as inclusions within hornblende. Zircon and apatite form euhedral disseminated crystals.

Anorthosite is largely medium-grained, consisting essentially of cumulate plagioclase (>80 vol.%) and minor pyroxene and amphibole. The accessory minerals include magnetite and ilmenite. Plagioclase shows random orientation with subequant to elongate crystals. The pyroxene occurs as intercumulus crystals of diopside.

Fine-grained gabbro represents the chilled marginal facies. It consists mainly of fine-grained equant plagioclase, clinopyroxene and orthopyroxene. The common accessories are magnetite and ilmenite, with a characteristic higher proportion compared to the coarse-grained gabbroic rocks. It shows a well-developed equigranular allotriomorphic texture. The texture and grain size are characteristic of a high cooling rate. There are no hydrous phases in this facies.

ANALYTICAL CONDITIONS

Based on the petrographic studies, nineteen fresh samples were selected for whole-rock chemical analyses. After crushing the whole sample, approximately 100 g of homogenous pebble-sized material was pulverized in an agate grinding bowl. Whole-rock XRF and ICP-MS analyses were performed at the GeoAnalytical Lab, Washington State University, USA. Concentrations of major element and trace elements were determined by combination of X-ray fluorescence (XRF) (ThermoARL X-ray Fluorescence Spectrometer) and solution-source Inductively-Coupled Plasma Mass Spectrometry (ICP-MS) (Agilent 7700). The analytical precision for XRF analyses, as calculated from duplicate samples, is better than 1 percent (2σ) for most major elements and better than 5 percent (2σ) for most trace elements (except Ni, Cr, Sc, V, and Cs). The complete XRF procedure and its analytical precision and detection limits are fully documented in Johnson and others (1999). Concentrations of REE as well as

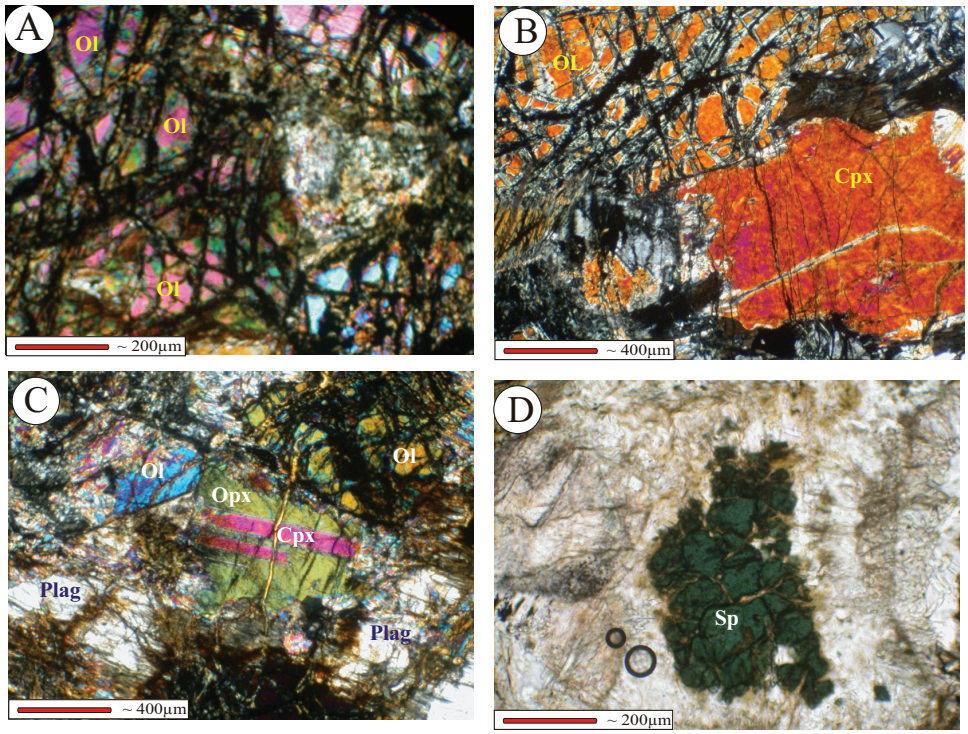

Fig. 4. Photomicrographs of the mafic and ultramafic rocks of the Dahanib intrusion. Abbreviations: Ol=olivine; Cpx=clinopyroxene, Opx=Orthopyroxene, Plag=plagioclase, Sp=spinel. (A) Abundant olivine crystal in dunite. (B) Olivine and clinopyroxene crystals with interstitial orthopyroxene in wehrlite. (C) Exsolution lamellae of clinopyroxene in orthopyroxene with intercumulus plagioclase intergrown with pyroxenes in lherzolite. (D) Clusters of green spinel (pleonaste) in lherzolite.

Ba, Th, Nb, Y, Hf, Ta, U, Pb, Rb, Cs, Sr, Sc and Zr were determined by ICP-MS. Analytical precision is better than ±5 percent (2σ) for most trace elements but for Th, U, Nb, Ta, Pb, Rb, Cs, Sc precision ranged between ±9 percent to ±17 percent (2σ).

Some representative samples of the Dahanib intrusion were selected to perform electron microprobe analysis of the following minerals: olivine, pyroxene, spinel, plagioclase and amphibole. Mineral analyses were performed at the Geological & Planetary Sciences (GPS) Division Analytical Facility, California Institute of Technology, using a five-spectrometer JEOL JXA-8200 electron microprobe. The analytical conditions were 15 kV accelerating voltage, 25 nA beam current, a focused beam (1 µm), 20 seconds on-peak counting times, a mix of natural (Amelia albite, Asbestos microcline) and synthetic (forsterite, fayalite, Mn-olivine, anorthite, NiO, TiO_2, Cr_2O_3) mineral standards, and the CITZAF matrix correction procedure. Mg# is Mg/(Mg + Fe^{2+}) atomic ratio and Fe^{3+}# is Fe^{3+}/(Cr + Al + Fe^{3+}) atomic ratio. We assumed all Fe as Fe^{2+} in silicates, and calculated Fe^{2+} and Fe^{3+} for spinel assuming stoichiometry. Cr# = molar Cr/(Cr + Al).

MINERAL COMPOSITIONS

Olivine

Olivine was analyzed from dunite, lherzolite, wehrlite, olivine websterite and olivine gabbronorite. Microprobe analyses of olivine and their calculated structural

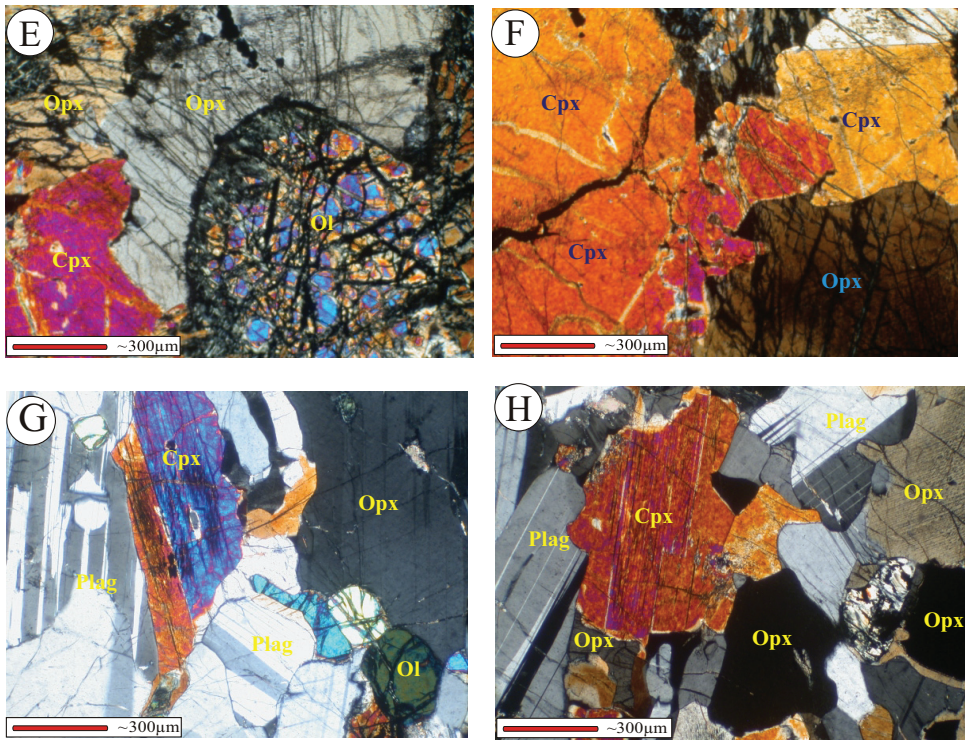

Fig. 4 (continued). (E) Pyroxenes and olivine in olivine websterite. (F) Cumulus clinopyroxene and orthopyroxene in websterite. (G) Olivine gabbronorite exhibiting a preferred orientation of the essential minerals. (H) Ophitic texture in gabbronorite.

formulae are shown in table 1SD (Supplementary Data, http://earth.geology.yale.edu/%7eajs/SupplementaryData/2017/Azer). The analyzed olivine crystals are compositionally unzoned, and forsterite content (Mg#) displays a systematic decrease from ultramafic to mafic rocks. The olivine of dunite has Fo content (0.86–0.88, av. 0.87) slightly higher than lherzolite (0.82–0.87; av. 0.85), wehrlite (0.82–0.85, av. 0.83), olivine websterite (0.80–0.82, av. 0.81) and olivine gabbronorite (0.78–0.81, av. 0.79). NiO and MnO contents are <0.3 weight percent (table 1SD).

The Fo and NiO contents of olivine from the studied rocks (0.78–0.88 and 0.04–0.30 wt.%, respectively) are lower than those recorded from ophiolites in the Eastern Desert (for example Khalil and Azer, 2007; Khalil and others, 2014; Gahlan and others, 2015; Obeid and others, 2016), but generally higher than those of the Alaskan-type intrusions (Helmy and El Mahallawi, 2003; Ahmed and others, 2008; Abd El-Rahman and others, 2012; Helmy and others, 2015), with some overlap. However, the Genina Gharbia mafic-ultramafic intrusion in the Eastern Desert, very close to Dahanib and considered to be an Alaskan-type intrusion, has high NiO contents in olivine (Helmy and others, 2014) similar to the Dahanib intrusion and other Egyptian layered intrusions (Essawy and others, 1997; Abdel-Halim and others, 2016). The NiO contents of olivine (<0.3 wt. %) are lower than that of the mantle olivine array (Takahashi and others, 1987), but similar to the Egyptian layered mafic intrusions (fig. 5A). On the same diagram, some of the analyzed olivine from the ultramafic rocks, especially dunite and lherzolite, overlap the field of fertile peridotites. Previously published data (Dixon, 1981a; Khedr and Arai, 2016) support the present results,

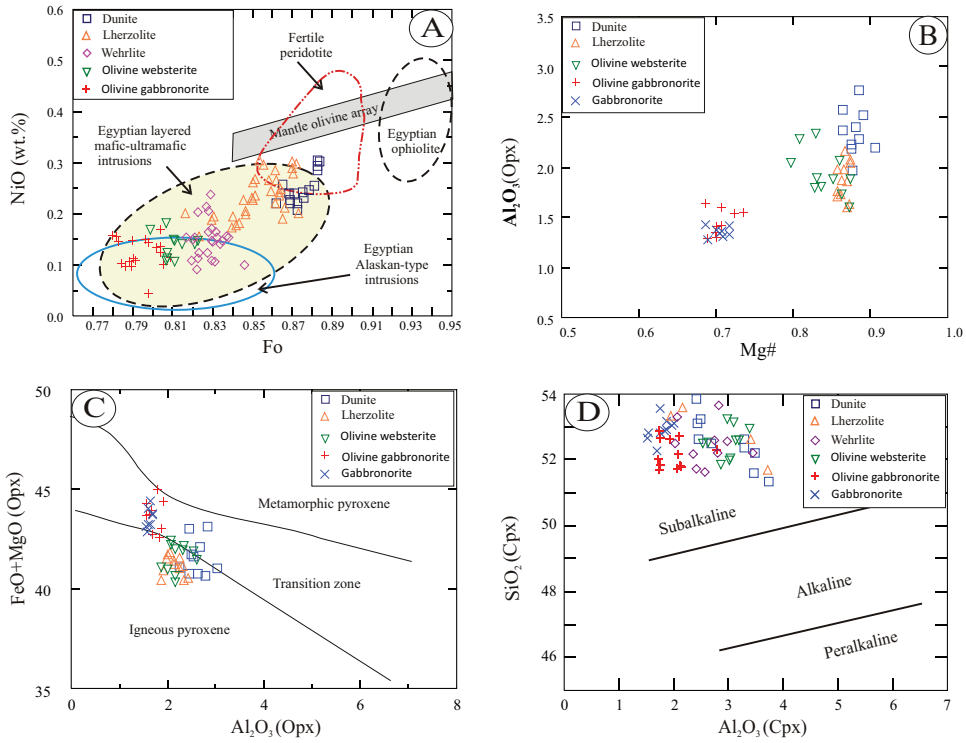

Fig. 5. (A) Variation of NiO (wt.%) and Fo contents of olivine in the Dahanib intrusion compared to the mantle olivine array (Takahashi and others, 1987); the field of Egyptian ophiolites based on data from Khudeir (1995a), Khalil and others (2014), Gahlan and others (2015) and Obeid and others (2016); the field of Egyptian layered intrusions from Essawy and others (1997) and Abdel-Halim and others (2016), and the field of Alaskan-type intrusion in Egypt from Khudeir (1995b), Helmy and El Mahallawi (2003), Ahmed and others (2008), Abd El-Rahman and others (2012) and Helmy and others (2015). (B) Mg# vs. Al_2O_3 of orthopyroxene in the Dahanib intrusion. (C) Classification of orthopyroxene analyses according to Rietmeijer (1983). (D) Classification of clinopyroxene analyses according to the SiO_2-Al_2O_3 discrimination diagram of Le Bas (1962).

although olivine associated with chromitite layers in the Dahanib intrusion has higher Fo (0.91–0.94) than olivine distant from chromitite. This can be attributed to the exchange of FeO and MgO under subsolidus conditions and should be separated from the discussion of primary magmatic compositions.

Pyroxenes

Both orthopyroxene and clinopyroxene were analyzed from the mafic and ultramafic rocks of the Dahanib intrusion. Orthopyroxene was analyzed from dunite, lherzolite, olivine websterite, olivine gabbronorite and gabbronorite (table 2SD, supplementary Data). The orthopyroxene shows a considerable variability of TiO_2 (0.05–0.2 wt. %), Al_2O_3 (1.3–2.7 wt.%), Cr_2O_3 (0.0–0.8 wt.%), CaO (0.2–1.0 wt.%) and MnO (0.14–0.8 wt.%). Their compositions plot close to the enstatite end-member of Morimoto and others (1988). There is a systematic change in composition from the ultramafic rocks (ternary projection $Wo_{0.4\text{-}1.9}En_{78.1\text{-}90.1}Fs_{11.0\text{-}20.3}$) to mafic rocks ($Wo_{1.0\text{-}1.9}En_{66.5\text{-}72.5}Fs_{26.5\text{-}31.5}$). Mg# of orthopyroxene decreases in ultramafic rocks (0.80–0.91) and then jumps down significantly to olivine gabbronorite and gabbronorite (0.69–0.74). Mg# in orthopyroxene is positively correlated with Al_2O_3 (fig.

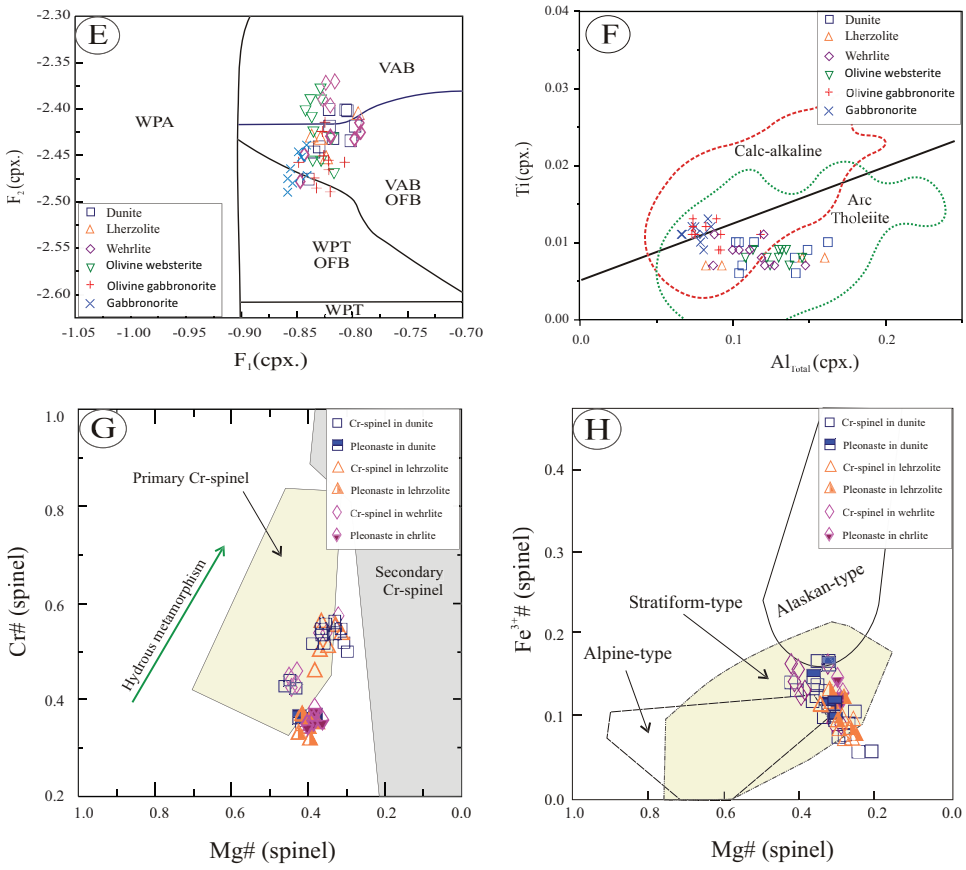

Fig. 5 (continued). (E) F1-F2 discrimination diagram for the composition of clinopyroxene (Nisbett and Pearce, 1977) (VAB: Volcanic arc basalt, OFB: Ocean floor basalt, WPT: Within-plate tholeiitic basalt, WPA: Within-plate alkali basalt), (F) Ti vs. Al plot for clinopyroxene (Leterrier and others, 1982). (G) Mg# versus Cr# diagram for Dahanib spinels (fields after Merlini and others, 2009; Grieco and Merlini, 2012). (H) Fe^{3+}# versus Mg# for Dahanib spinels; the fields of the different types of mafic–ultramafic complexes are from Kepezhinskas and others (1993).

5B), as expected for a fractional crystallization sequence. On the MgO+FeO versus Al_2O_3 diagram (Rietmeijer, 1983), orthopyroxene from the ultramafic rocks plots mainly in the igneous field, while orthopyroxene from the olivine gabbronorite and gabbronorite plots mainly in the transition zone between igneous and metamorphic rocks (fig. 5C). Orthopyroxene analyses in the transition zone may reflect subsolidus re-equilibration during cooling or magmatic crystallization under lower pressure than in the ultramafic rocks.

Clinopyroxene was analyzed from dunite, lherzolite, wehrlite, olivine websterite, olivine gabbronorite and gabbronorite (table 3SD, supplementary Data). Two generations of clinopyroxene are found in the ultramafic rocks. The earlier generation comprises large crystals and the later one occurs as exsolved lamellae in orthopyroxene. We restricted our analyses to the earlier generation. All clinopyroxene from the Dahanib rock units is diopsidic in composition with a high wollastonite component (43–49%) and relatively low Al_2O_3 (1.5–3.7 wt %) and TiO_2 (0.23–0.49 wt %). Augite is not found. The clinopyroxene of ultramafic rocks has wollastonite contents between

44 and 50 mole percent, whereas that of the mafic rocks have lower wollastonite contents (43–47 mole %). The concentration of Al_2O_3 in clinopyroxene from the olivine gabbronorite and gabbronorite is relatively low (av. 1.9 wt. %) compared to the ultramafic rocks (av. 2.9 wt.%), consistent with appearance of plagioclase in the fractionating assemblage early in the mafic sequence. Clinopyroxene from the ultramafic varieties has higher Mg# (0.85-0.91) than the olivine gabbronorite and gabbronorite (0.80–0.83 and 0.76–0.80, respectively). Similar compositions are reported for clinopyroxene from layered mafic-ultramafic intrusions in the Eastern Desert and Sinai (Azer and El-Gharbawy, 2011; Abdel Halim and others, 2016).

Pyroxene plays an important role in igneous petrogenetic studies (Le Bas, 1962; Nisbett and Pearce, 1977; Leterrrier and others, 1982). On the SiO_2 versus Al_2O_3 diagram of Le Bas (1962), all clinopyroxene analyses plot in the subalkaline field (fig. 5D). On the F_1-F_2 discrimination diagram of Nisbett and Pearce (1977), they cross from the volcanic-arc field towards the ocean floor basalt field, avoiding within-plate fields (fig. 5E). The sub-alkaline arc tholeiite affinity is supported by plotting the pyroxene analyses on the Al vs. Ti diagram of Leterrrier and others (1982) (fig. 5F).

Spinel

Spinel was analyzed from dunite, lherzolite and wehrlite. The chemical analyses and structural formulae of spinel are given in table 4SD (Supplementary Data). The compositions of spinel are widely variable. Variability is evident even among crystals within a given thin section. Based on petrographic observation and mineral analyses, two types of spinel can be recognized: Cr-spinel and Al-spinel (pleonaste). Cr-spinel occurs as a cumulate phase or as a dispersed accessory mineral. Pleonaste occurs only as an accessory phase; it appears somewhat later in the crystallization sequence than Cr-spinel.

Cr-spinel has a wide-range of Al_2O_3 (18.5–28.8 wt.%), Cr_2O_3 (29.3–40.3 wt.%) and MgO (7.1–13.2 wt.%) contents. Pleonaste has higher Al_2O_3 (30.0–35.5 wt.%) than Cr_2O_3 (24.3–28.0 wt.%). Cr# in pleonaste (0.32–0.37) is less than in Cr-spinel (0.41–0.57). The analyzed spinel is mainly of primary magmatic origin based on rigorous petrography and chemistry (Cr#-Mg# plot; fig. 5G). However, variations observed among the chemical compositions of spinel can be attributed to sub-solidus re-equilibration with adjacent silicate minerals and exsolution (Azer and Stern, 2007; Bilqees and others 2016). The compositions of spinel in the Dahanib intrusion have chemical characteristics in the Fe^{3+}#-Mg# diagram (Kepezhinskas and others, 1993) similar to spinel from stratiform complexes, which are clearly distinguished from those of ophiolitic (alpine-type) and Alaskan-type complexes (fig. 5H).

Plagioclase

Results of chemical analyses of plagioclase from the Dahanib intrusion are presented in table 5SD (Supplementary Data, http://earth.geology.yale.edu/%7eajs/SupplementaryData/2017/Azer). The analyzed plagioclase shows a wide range of An-contents, An_{40} to An_{85}. The plagioclase is homogenous within individual specimens. The plagioclase of ultramafics from the Dahanib intrusion is mainly bytownite (An_{80} to An_{85}), whereas that of the olivine gabbronorite ranges from andesine to bytownite (An_{40}-An_{82}) and in gabbronorite it ranges from andesine to labradorite (An_{40}-An_{70}). Dixon (1981a) recognized nearly similar high-An plagioclase (An_{79} to An_{94}) in the Dahanib intrusion, mainly bytownite with rare anorthite. On the other hand, Khedr and Arai (2016) recognized only low-An plagioclase (An_{26} to An_{54}) in the same intrusion. By contrast, we have found both ranges, although no specimens as sodic as the most sodic analyses reported by Khedr and Arai (2016) and no specimens as calcic as the most calcic analyses reported by Dixon (1981a). Generally, the

anorthite-rich plagioclase of the Dahanib intrusion is characteristic of cumulate rocks (Arculus and Wills, 1980; Beard, 1986).

Amphiboles

Chemical analyses of the amphiboles in the Dahanib intrusion are shown in table 6SD (Supplementary Data). Most of the analyzed amphiboles in the ultramafic rocks are secondary amphiboles after pyroxenes, while primary amphiboles are recorded only in the gabbros as minor phase. According to the classification of Leake and others (1997), the amphibole is calcic and most of them have A-site occupancy (Na+K) < 0.5 atoms per formula unit (apfu). The primary amphibole is rich in TiO_2 and classified as tschermakite, tschermakitic hornblende, magnesio-hornblende or pargasitic hornblende. The secondary amphibole is depleted in TiO_2 and classified as tremolite, tremoltic hornblende or anthophyllite.

WHOLE-ROCK GEOCHEMISTRY

Whole-rock XRF and ICP-MS analyses for 19 samples from the Dahanib intrusion (10 ultramafics and 9 mafics) are given in tables 2 and 3. The analyzed samples vary widely in their composition and have low values of loss on ignition (LOI < 2.2 wt.%) due to their low degree of alteration. The ultramafic rocks are depleted in alkalis and alumina, but have high MgO, Fe_2O_3, Cr and Ni, reflecting the high proportion of ferromagnesian silicates and the low proportions of plagioclase. The dunite has the lowest SiO_2 contents (<39 wt.%) and the highest MgO contents (43.0–43.8 wt.%). MgO contents in the ultramafic rocks decrease with increasing silica from dunite to pyroxenite. The pyroxenite has the highest Al_2O_3 (8.9–9.4 wt.%) and CaO (14.8–16.7 wt.%) among the ultramafic rocks. TiO_2 contents of the ultramafic rocks do not correlate with either MgO or CaO contents and are fairly low (<0.81 wt.%). Mg# varies in the ultramafics based on rock type (0.86–0.87 in dunite, 0.85–0.86 in lherzolite, 0.84–0.85 in wehrlite and 0.73–0.78 in pyroxenite). Mg# of the olivine-rich ultramafic rocks (0.84–0.87) is consistent with averaging over the olivine composition in each sample (0.82–0.89).

Among the analyzed mafic samples, the olivine gabbronorite has SiO_2 contents (45.0 wt.%) similar to those of the pyroxenite (45.5–46.6 wt.%), whereas the gabbronorite ranges somewhat higher (45.6–49.6 wt.% SiO_2). The mafic rocks show a wide spectrum of MgO contents, 16.3 weight percent in olivine gabbronorite and from 6.6 to 8.2 weight percent in the gabbronorite. Al_2O_3 content increases from the olivine gabbronorite (13.3 wt.%) to the gabbronorite (16.6–18.4 wt.%). CaO also correlates negatively with MgO. On the other hand, the FeO, Cr and Ni contents decrease with decreasing MgO. These trends are broadly consistent with fractionation/accumulation of olivine, spinel and pyroxenes. The Mg# is 0.73 in the analyzed olivine gabbronorite and varies from 0.60 to 0.64 in the gabbronorite samples.

Using the TAS classification diagram of Cox and others (1979), the Dahanib gabbronorites plot within the gabbro field (fig. 6A), and below the alkalic–sub-alkalic boundary line of Miyashiro (1978). The sub-alkaline character of the Dahanib intrusion is also indicated by the low Nb/Y ratios (<0.3) in all rock units, and the high SiO_2 and low Al_2O_3 contents of the clinopyroxene (fig. 5D). The gabbroic rocks of the Dahanib intrusion plot near the beginning of the medium-K calk-alkaline differentiation trend (fig. 6B). However, the low ratios of Zr/Y (1.4-3.7), La/Yb (1.0-2.3) and Th/Yb (0.2-0.7) in the Dahanib intrusion support a tholeiitic affinity for the parental magmas (Barrett and MacLean, 1999). Bulk chemistry corroborates the cumulate nature evident from petrographic examination of the studied rocks; on the AFM diagram of Beard (1986), the mafic and ultramafic rocks plot in the arc-related cumulate fields (fig. 6C).

Table 2

Major oxide and trace element contents of the mafic and ultramafic rocks of the Dahanib intrusion

Rock type	Ultramafic						
	Dunite			Lherzolite		Wehrlite	
Sample No.	DH7	DH10	DH15	DH18	DH26	DH13	DH45
Major oxides (wt.%)							
SiO_2	38.66	38.97	39.45	42.05	43.07	39.73	41.01
TiO_2	0.17	0.18	0.08	0.15	0.16	0.09	0.08
Al_2O_3	1.24	1.37	2.44	2.86	3.92	1.17	1.87
Fe_2O_3	13.17	14.05	12.81	12.44	12.38	12.92	12.76
MnO	0.22	0.21	0.15	0.2	0.18	0.17	0.18
MgO	43.82	42.98	39.34	36.01	35.16	38.08	35.02
CaO	0.56	0.71	3.37	3.63	3.41	5.64	6.96
Na_2O	0.07	0.08	0.16	0.17	0.14	0.08	0.07
K_2O	0.05	0.06	0.08	0.03	0.03	0.02	0.01
P_2O_5	0.01	0.03	0.03	0.01	0.02	0.01	0.02
LOI	2.01	1.51	1.71	1.81	1.38	1.98	1.46
Total	99.98	100.15	99.62	99.36	99.85	99.89	99.44
Trace elements (ppm)							
Ni	893	911	854	733	747	1016	1001
Cr	2274	2663	2301	2066	2143	2006	1769
Sc	18.2	18.9	20.8	30.1	29.3	11.5	13.7
V	84	67	75	100	108	71	63
Ba	26	21	31	58	56	49	44
Rb	2.5	2.2	2.6	2.8	3.6	3.1	2.8
Sr	29	41	64	66	78	16	21
Zr	7.4	7.1	9.9	12.4	11.5	4.6	3.3
Y	2.6	2.2	7.2	6.3	3.3	2.1	1.7
Nb	0.2	0.2	0.2	0.2	0.3	0.4	0.3
Ga	3.3	2.4	3.8	5.1	6.2	1.8	2.1
Cu	102	121	135	92	89	108	79
Zn	82	74	78	112	117	92	81
Pb	1.8	1.3	2.2	2.4	2.7	1.9	2.3
Th	0.1	0.2	0.1	0.1	0.1	0.1	0.2
U	0.3	0.1	0.2	0.2	0.2	0.1	0.2
Cs	0.2	0.4	0.5	0.1	0.6	0.2	0.1
Ta	0.04	0.05	0.06	0.07	0.06	0.04	0.05
Hf	0.4	0.3	0.5	0.6	0.5	0.5	0.6
Geochemical parameters							
Mg#	0.87	0.86	0.86	0.85	0.85	0.85	0.84
Zr/Y	2.85	3.23	1.38	1.97	3.48	2.19	1.94
Th/Nb	0.50	1.00	0.50	0.50	0.33	0.25	0.67
Th/Ta	2.50	4.00	1.67	1.43	1.67	2.50	4.00
Ta/Hf	0.10	0.17	0.12	0.12	0.12	0.08	0.08
Ba/Nb	130	105	155	290	186	122	146
Th/Yb	0.43	0.67	0.53	0.67	0.45	0.38	0.59
Nb/Y	0.08	0.09	0.03	0.03	0.09	0.19	0.18
Nb/Yb	0.43	0.33	1.05	1.33	1.36	2.31	1.47
Ce/Pb	0.39	0.61	0.54	0.39	0.40	0.73	0.68

N-MORB-normalized multi-element spider diagrams of the mafic and ultramafic samples of the Dahanib intrusion, using the normalizing values of Pearce (1983), are shown in figure 7 (A and B). The ultramafic rocks show mostly parallel N-MORB normalized patterns except for pyroxenites, which are more enriched in Sr, K and Ti than peridotites. The ultramafic rocks are characterized by pronounced enrichment in Rb, Ba and Th. Wehrlite samples have small negative anomalies in Nb, Zr, and Ti. The

TABLE 2
(continued)

Rock type	Ultramafic			Mafic		
	Pyroxenite			Olivine gabbronorite	gabbronorite	
	Olivine websterite		Websterite			
Sample No.	DH29	DH40	DH42	DH44	DH21	DH24
Major oxides (wt.%)						
SiO_2	46.63	45.57	45.52	45.04	49.36	49.37
TiO_2	0.54	0.77	0.81	0.75	0.76	0.61
Al_2O_3	9.02	8.92	9.37	13.32	16.85	16.89
Fe_2O_3	10.57	9.04	11.72	11.72	8.95	8.57
MnO	0.13	0.19	0.16	0.14	0.09	0.09
MgO	16.97	16.59	15.71	16.33	7.28	6.87
CaO	15.44	16.71	14.78	10.76	10.81	11.08
Na_2O	0.08	1.08	1.01	1.06	2.39	2.67
K_2O	0.24	0.32	0.27	0.29	0.63	0.76
P_2O_5	0.02	0.01	0.01	0.03	0.05	0.04
LOI	0.53	0.42	0.28	1.07	2.15	2.21
Total	100.17	99.62	99.64	100.51	99.32	99.16
Trace elements (ppm)						
Ni	265	193	214	274	136	104
Cr	623	598	602	527	484	341
Sc	31.4	39.2	40.7	31.3	23.8	15.7
V	214	253	198	162	123	146
Ba	45	51	48	34	92	116
Rb	3.1	2.8	3.9	5.3	8.7	11.2
Sr	76	85	96	331	358	318
Zr	20.7	19.4	22.5	21.2	37.1	42.3
Y	5.6	5.7	6.1	8.1	11.5	15.4
Nb	0.3	0.5	0.4	0.9	1.3	1.4
Ga	1.2	1.3	0.9	12.6	16.3	16.1
Cu	19	26	31	125	117	43
Zn	48	51	36	83	55	67
Pb	2.5	3.1	2.7	3.6	0.6	0.6
Th	0.2	0.1	0.2	0.3	0.3	0.5
U	0.1	0.2	0.2	0.4	0.3	0.3
Cs	0.2	0.1	0.3	0.3	0.2	0.4
Ta	0.05	0.06	0.07	0.06	0.11	0.12
Hf	0.7	0.6	0.6	0.6	1.4	1.3
Geochemical parameters						
Mg#	0.76	0.78	0.73	0.73	0.62	0.61
Zr/Y	3.70	3.40	3.69	2.62	3.23	2.75
Th/Nb	0.67	0.20	0.50	0.33	0.23	0.36
Th/Ta	4.00	1.67	2.86	5.00	2.73	4.17
Ta/Hf	0.07	0.10	0.12	0.10	0.08	0.09
Ba/Nb	150	102	120	37	70	82
Th/Yb	0.49	0.28	0.56	0.38	0.18	0.31
Nb/Y	0.05	0.09	0.07	0.11	0.11	0.09
Nb/Yb	0.73	1.39	1.11	1.13	0.77	0.86
Ce/Pb	0.71	0.64	0.62	1.05	10.27	12.08

mafic samples also have mostly parallel N-MORB-normalized patterns and are characterized by enrichment in LILE (that is, K, Rb, Ba, Th), depletion in HFSE relative to N-MORB, and nearly flat HFSE except for negative Ti anomalies in all gabbronorite samples except the lowest-SiO_2 sample. The incompatible trace element contents (except Ti) in the mafic rocks show a systematic increase from olivine gabbronorite to gabbronorite (fig. 7B). The depletion in Ta and Nb relative to the LILE seen in the mafic samples is a common geochemical feature of late-orogenic to post-collisional

Table 2
(continued)

Rock type	Mafic gabbronorite					
Sample No.	DH29	DH31	DH37	DH48	DH51	DH56
Major oxides (wt.%)						
SiO_2	49.71	45.64	46.62	47.66	48.34	48.61
TiO_2	0.72	0.97	0.79	0.81	0.71	0.67
Al_2O_3	16.76	18.41	18.31	16.72	17.04	16.56
Fe_2O_3	8.93	9.76	9.81	10.07	8.74	9.88
MnO	0.14	0.08	0.06	0.08	0.13	0.1
MgO	6.63	8.24	7.94	7.65	7.93	7.62
CaO	10.73	12.46	11.52	11.65	10.72	11.24
Na_2O	2.74	2.14	2.32	2.46	2.56	2.44
K_2O	0.73	0.44	0.54	0.58	0.66	0.59
P_2O_5	0.05	0.08	0.07	0.05	0.06	0.04
LOI	1.09	1.7	1.02	1.73	2.1	1.08
Total	98.23	99.92	99.00	99.46	98.99	98.83
Trace elements (ppm)						
Ni	96	166	145	143	99	121
Cr	352	518	478	501	327	478
Sc	14.4	36.2	29.7	21.5	18.3	24.6
V	92	273	261	184	96	137
Ba	102	80	49	54	94	82
Rb	10.3	6.2	7.6	6.8	6.5	7.5
Sr	328	459	447	433	414	403
Zr	57.2	27.4	24.6	28.3	33.4	32.4
Y	18.7	10.3	11.9	9.5	14.6	12.5
Nb	1.5	1.3	1.1	1.2	1.4	1.3
Ga	14.7	17.3	15.5	16.1	15.3	14.8
Cu	37	184	172	83	31	94
Zn	45	68.2	42	63	38	43
Pb	0.3	0.6	0.9	1.1	0.8	1.4
Th	0.4	0.3	0.4	0.3	0.4	0.5
U	0.5	0.4	0.7	0.3	0.5	0.3
Cs	0.2	0.3	0.6	0.4	0.3	0.5
Ta	0.13	0.08	0.09	0.12	0.1	0.11
Hf	1.6	0.7	0.8	0.7	1.1	0.9
Geochemical parameters						
Mg#	0.60	0.63	0.62	0.60	0.64	0.60
Zr/Y	3.06	2.66	2.07	2.98	2.29	2.59
Th/Nb	0.27	0.23	0.36	0.25	0.29	0.38
Th/Ta	3.08	3.75	4.44	2.50	4.00	4.55
Ta/Hf	0.08	0.11	0.11	0.17	0.09	0.12
Ba/Nb	68	61	44	45	67	63
Th/Yb	0.21	0.26	0.31	0.25	0.29	0.32
Nb/Y	0.08	0.13	0.09	0.13	0.10	0.10
Nb/Yb	0.77	1.12	0.86	0.99	1.01	0.84
Ce/Pb	26.90	7.28	5.39	5.03	7.26	4.55

Mg# is molar Mg/(Mg+Fe), calculated assuming total Fe as FeO.

magmas of the ANS (for example Azer and others, 2012; Khalil and others, 2015; Abdel Halim and others, 2016). The negative Ti anomaly in the high-silica gabbronorites may be attributed to fractionation of Fe-Ti oxides. It is curious that the overall trace element patterns of the ultramafic and mafic samples are nearly parallel to one another and, in particular, that the most incompatible large ion lithophile elements are so enriched in the ultramafics. This likely reflects a component of trapped melt within the cumulates, perhaps also visible for example as clinopyroxene in the dunites and plagioclase in the wehrlites.

TABLE 3

Rare earth element contents of the mafic and ultramafic rocks of the Dahanib intrusion

Rock type	Ultramafics						
	Dunite		Lherzolite			Wehrlite	
Sample No.	DH7	DH10	DH15	DH18	DH26	DH13	DH45
La	0.27	0.31	0.44	0.28	0.36	0.49	0.54
Ce	0.71	0.79	1.19	0.94	1.08	1.39	1.57
Pr	0.11	0.13	0.18	0.14	0.17	0.21	0.27
Nd	0.56	0.62	0.89	0.84	1.02	1.17	1.51
Sm	0.18	0.19	0.25	0.22	0.33	0.37	0.49
Eu	0.08	0.11	0.09	0.09	0.13	0.16	0.19
Gd	0.26	0.28	0.29	0.25	0.42	0.46	0.59
Tb	0.05	0.05	0.05	0.04	0.07	0.08	0.1
Dy	0.33	0.38	0.34	0.22	0.45	0.49	0.65
Ho	0.07	0.08	0.07	0.05	0.08	0.11	0.14
Er	0.21	0.28	0.19	0.14	0.23	0.29	0.37
Tm	0.03	0.04	0.03	0.02	0.03	0.04	0.05
Yb	0.23	0.3	0.19	0.15	0.22	0.26	0.34
Lu	0.03	0.04	0.03	0.02	0.03	0.04	0.05
Sum	**3.12**	**3.60**	**4.23**	**3.40**	**4.62**	**5.56**	**6.86**
Eu/Eu*	1.13	1.46	1.02	1.17	1.07	1.19	1.08
$(La/Yb)_n$	0.79	0.70	1.57	1.26	1.11	1.27	1.07
$(La/Sm)_n$	0.95	1.03	1.11	0.80	0.69	0.84	0.70
$(Gd/Lu)_n$	1.06	0.86	1.18	1.53	1.72	1.41	1.45
$(Ce/Yb)_n$	0.80	0.68	1.62	1.62	1.27	1.38	1.20
$(La/Lu)_n$	0.92	0.79	1.50	1.43	1.23	1.26	1.11
La/Yb	1.17	1.03	2.32	1.87	1.64	1.88	1.59

The REE analyses of 19 samples from the Dahanib intrusion are given in table 3 and their chondrite-normalized REE patterns are represented in figure 7 (C and D). The Dahanib rocks have variable ΣREE contents, reflecting different abundances and compositions of intercumulus liquids. The chondrite-normalized REE patterns of the ultramafics are almost flat (fig. 7C). Gabbronorites also have generally flat REE patterns (fig. 7D) and most have small positive Eu anomalies (Eu/Eu* = 0.94-1.30). The olivine gabbronorite is enriched in LREE relative to HREE [$(La/Lu)_N$ = 1.21], with generally flat LREE [$(La/Sm)_N$ = 0.91] and visibly fractionated HREE [$(Gd/Lu)_N$ = 1.39]. It has a positive Eu anomaly (Eu/Eu* = 1.27).

DISCUSSION

Understanding the origin and evolution of the Late Neoproterozoic mafic-ultramafic complexes in the Eastern Desert of Egypt will provide important constraints for reconstructing the geodynamic evolution of the ANS and the other Neoproterozoic orogenic belts, yet the petrogenesis of these rocks has been the subject of much debate. Field studies, mineral compositions and bulk chemistry of the Dahanib intrusion indicate that it is neither deformed nor metamorphosed and preserves much evidence of its primary origin. It intrudes metamorphic rocks and deformed calc-alkaline syntectonic granodiorite, which indicates that it is younger than both of those units.

Table 3
(continued)

Rock type	Ultramafic			Mafic		
	Pyroxenite			Olivine gabbronorite	Gabbronorite	
	Olivine websterite		Websterite			
Sample No.	DH29	DH40	DH42	DH44	DH21	DH24
La	0.68	0.73	0.59	1.42	2.36	2.77
Ce	1.77	1.99	1.67	3.78	6.16	7.25
Pr	0.28	0.29	0.27	0.59	0.98	1.15
Nd	1.41	1.52	1.29	2.92	5.09	5.81
Sm	0.46	0.44	0.411	0.98	1.72	1.85
Eu	0.15	0.15	0.14	0.48	0.69	0.74
Gd	0.49	0.47	0.45	1.36	2.29	2.31
Tb	0.09	0.09	0.08	0.22	0.38	0.41
Dy	0.62	0.54	0.53	1.38	2.62	2.66
Ho	0.14	0.11	0.12	0.29	0.56	0.56
Er	0.42	0.36	0.35	0.81	1.63	1.58
Tm	0.06	0.05	0.05	0.12	0.25	0.24
Yb	0.41	0.36	0.36	0.8	1.69	1.62
Lu	0.06	0.05	0.05	0.12	0.25	0.24
Sum	**7.04**	**7.15**	**6.36**	**15.27**	**26.67**	**29.19**
Eu/Eu*	0.97	1.01	0.99	1.27	1.06	1.09
$(La/Yb)_n$	1.12	1.37	1.11	1.20	0.94	1.16
$(La/Sm)_n$	0.93	1.05	0.91	0.91	0.86	0.95
$(Gd/Lu)_n$	1.00	1.15	1.10	1.39	1.12	1.18
$(Ce/Yb)_n$	1.12	1.43	1.20	1.22	0.94	1.16
$(La/Lu)_n$	1.16	1.50	1.21	1.21	0.97	1.18
La/Yb	1.66	2.03	1.64	1.78	1.39	1.71

The Dahanib intrusion was emplaced after the bulk of subduction-related magmatism and deformation ended in the area (El-Ramly, 1972; El-Gaby and others, 1990; Meguid and El-Metwally, 1998). Accordingly, it could represent either a late calc-alkaline phase or a post-collisional magmatic phase. The lack of detailed field studies and the contradictory results of previous mineralogical and petrological studies of the Dahanib intrusion have permitted conflicting interpretations of its likely petrogenetic and tectonic development. Based on the data presented here, in the following sections we will try to assess the tectonic setting, sources and magmatic processes that were responsible for generation and evolution of the Dahanib intrusion. Also, we will use the available data to settle whether the Dahanib intrusion is best described as an Alaskan-type complex or a layered intrusion.

Tectonic Setting

The intrusive contacts of the Dahanib intrusion with country rocks clearly suggest that it is not a fragment of an ophiolite. The field relationship of the Dahanib intrusion with the surrounding rocks suggests an age younger than 710 Ma, which is the age of the surrounding quartz-diorite (Dixon, 1981b). Also, field investigations reveal that the Dahanib rocks are largely undeformed and unmetamorphosed, excluding any

TABLE 3
(continued)

Rock type	Mafic					
	Gabbronorite					
Sample No.	DH29	DH31	DH37	DH48	DH51	DH56
La	3.14	1.71	1.92	2.14	2.29	2.49
Ce	8.07	4.37	4.85	5.53	5.81	6.37
Pr	1.32	0.69	0.75	0.86	0.91	1.02
Nd	6.55	3.48	3.79	4.38	4.65	4.91
Sm	2.14	1.25	1.32	1.45	1.55	1.66
Eu	0.76	0.61	0.56	0.64	0.66	0.67
Gd	2.83	1.65	1.69	1.77	1.98	2.15
Tb	0.47	0.28	0.29	0.3	0.34	0.37
Dy	3.03	1.78	1.89	1.97	2.25	2.46
Ho	0.65	0.39	0.41	0.42	0.48	0.54
Er	1.83	1.12	1.22	1.19	1.37	1.54
Tm	0.29	0.17	0.19	0.18	0.21	0.23
Yb	1.94	1.16	1.28	1.21	1.39	1.55
Lu	0.3	0.18	0.2	0.19	0.21	0.23
Sum	**33.32**	**18.84**	**20.36**	**22.23**	**24.10**	**26.19**
Eu/Eu*	0.94	1.30	1.15	1.22	1.15	1.08
$(La/Yb)_n$	1.09	1.00	1.01	1.20	1.11	1.09
$(La/Sm)_n$	0.93	0.86	0.92	0.93	0.93	0.95
$(Gd/Lu)_n$	1.16	1.12	1.04	1.14	1.16	1.15
$(Ce/Yb)_n$	1.08	0.98	0.98	1.18	1.08	1.06
$(La/Lu)_n$	1.07	0.97	0.98	1.15	1.12	1.11
La/Yb	1.62	1.47	1.50	1.77	1.65	1.61

Concentrations in ppm.
Subscript n indicates normalization to chondritic ratio according to Sun and McDonough (1989).
Eu* is the expected Eu based on the geometric average of Sm and Gd concentrations and the chondritic relative abundances of Sm, Eu, and Gd.

correlation to the early stage of subduction-related activity preserved as metamorphosed rocks in the Eastern Desert. Instead the Dahanib intrusion must belong to the late-orogenic or post-collision magmatic phase (<650 Ma), which has been shown to encompass a transition in the tectonic setting from compression to extension (Genna and others, 2002; Johnson and others, 2011). Unfortunately, we do not have evidence to provide a lower-bound age or to say how long after the end of collision the intrusion took place.

The cumulate nature of the Dahanib intrusion may obscure the signature of major and trace elements of the parent magma. Therefore, we cannot apply a number of bulk-chemistry-based tectonic discrimination diagrams intended for volcanic rocks. However, some aspects of liquid chemistry are faithfully inherited by cumulates derived from them. The gabbroic samples have high Zr/Y ratios suggesting a continental arc environment at a convergent plate boundary (Wilson, 1994). This is consistent with the Th/Yb vs. Nb/Yb signature (fig. 8A), where they plot in the field of continental arcs (Pearce and Peate, 1995). Although the mafic-ultramafic rocks of the Dahanib intrusion share many geochemical characteristics with subduction-related magmas such as enrichment of LILE and slightly negative Nb-Ta anomalies, these

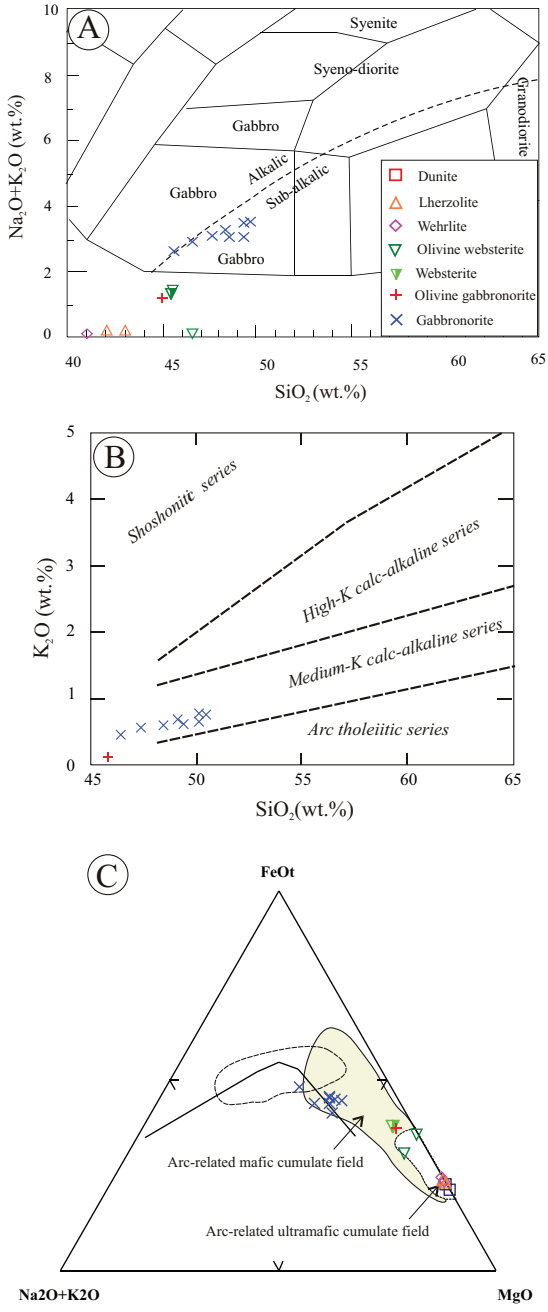

Fig. 6. Whole-rock major element chemistry of the Dahanib intrusion. (A) TAS diagram (Cox and others, 1979; adapted by Wilson, 1994). The dividing line (dashed) between alkalic and sub-alkalic magma series is from Miyashiro (1978). (B) SiO_2-K_2O diagram (after Rickwood, 1989). (C) AFM diagram for ultramafic–mafic lithologies with fields of arc-related cumulate ultramafic–mafic rocks and arc-related gabbro and diorite fields from Beard (1986).

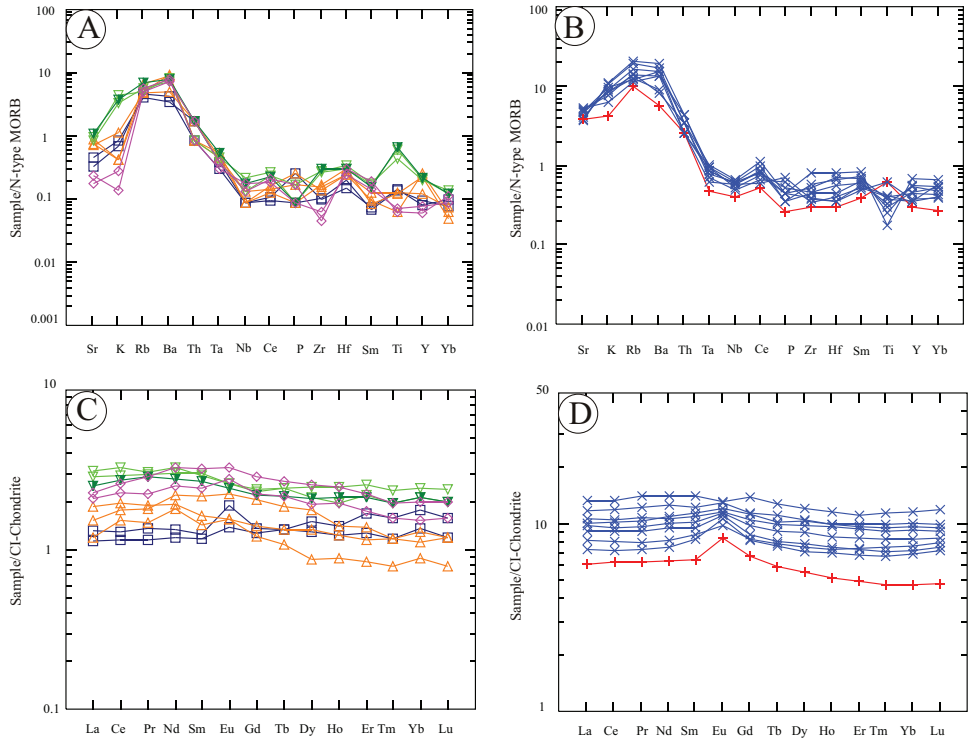

Fig. 7. Normalized whole-rock multi-trace element diagrams for Dahanib intrusion samples. N-MORB-normalized extended spider diagrams for (A) ultramafic samples and (B) mafic samples. Chondrite-normalized REE patterns for (C) ultramafic samples and (D) mafic samples. MORB and chondrite normalization values after Pearce (1983) and Sun and McDonough (1989), respectively. Colors and symbols correspond to rock types as shown in the legend of fig. 6A.

geochemical features often persist into post-orogenic settings (for example, Saunders and others, 1980; Pearce, 1983; Wilson, 1994; Hollings and Wyman, 1999; Gill, 2010). The subduction geochemical signature may be inherited from lithospheric mantle that was modified by a previous subduction event, as argued recently for the sources of other Neoproterozoic post-collisional mafic magmas in the ANS (Azer and others, 2012; Khalil and others, 2015).

The cumulate versus volcanic distinction can be avoided by focusing on mineral rather than whole-rock chemistry. We showed above that the magmatic affinity of pyroxenes (Le Bas, 1962; Nisbett and Pearce, 1977; Leterrier and others, 1982) confirms a sub-alkaline parental magma with mainly tholeiitic character (figs. 5D and 5F).

Genesis of the Parental Magma

Several approaches are used to estimate the compositions of parental magmas of mafic–ultramafic rocks. The slight enrichment in LILE and depletion in HFSE (Nb, Ta and Ti) of the Dahanib intrusion is consistent with a late- to post-orogenic environment in the ANS since these features are inherited from a previous subduction process (Khalil and others, 2015; Abdel Halim and others, 2016). Magmatic evolution in such settings can be controlled by a range of processes including various degrees of partial melting in the source, various extents of crystal fractionation in the magmatic system,

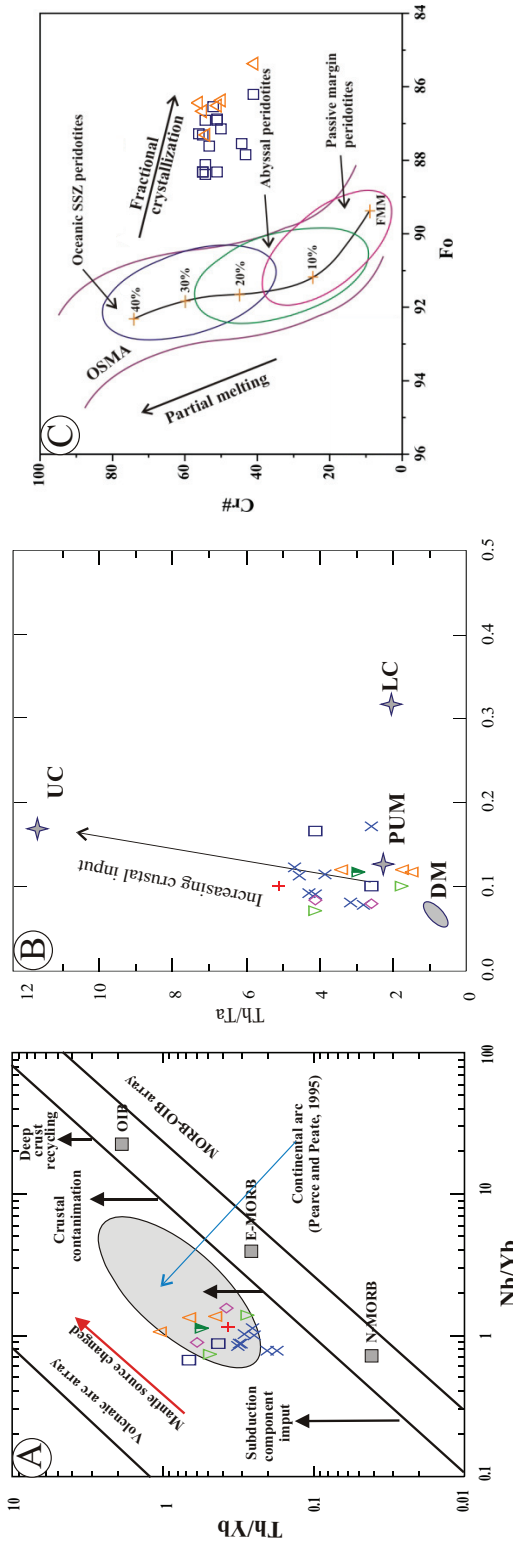

Fig. 8. Discrimination diagrams for mantle and crustal components. (A) Th/Yb vs. Nb/Yb diagram with fields and arrows indicating various types of contamination of primitive mantle sources (after Pearce, 2008 and Scandolara and others, 2014). (B) Ta/Hf vs. Th/Ta diagram comparing the Dahanib intrusion to depleted mantle [DM, after Salters and Stracke (2004) and Workman and Heart (2005)], the primitive upper mantle [PUM, after McDonough and Sun (1995)], and upper (UC) and lower (LC) continental crust values after Rudnick and Gao (2003). (C) Compositional variation of Cr# of Cr-spinel and Fo content of olivine in spinel-olivine pairs. Olivine-spinel mantle array (OSMA) and melting trend are from Arai (1994). Field of abyssal peridotites after Dick and Bullen (1984); fields of supra-subduction zone and passive margin peridotites after Pearce and others (2000). Symbols as in legend of fig. 6A.

or a combination of these two mechanisms (Jagoutz, 2014). We may isolate the source-related processes by focusing either on the chilled margin facies, which is most likely to represent a liquid composition, or on the dunite, the most primitive rock in the Dahanib intrusion, with the highest Mg# olivine, and most likely to reflect early crystallization from the parental melt of the intrusion. The dominance of olivine and spinel at the earliest phase of crystallization requires a parental melt rich in MgO and poor in SiO_2. Below we will model both the primitive melt and the fractionation sequence using the chilled margin facies, showing that it is compatible with forming the observed dunite as an early (but not quite primary) fractionating assemblage.

All the Dahanib rocks have nearly similar chondrite-normalized REE patterns, suggesting that they were derived from the same source. The limited variation of LILE and the absence of any Ce anomalies suggest a mantle source rather than any crustal anatexis (for example, Neal and Taylor, 1989; Class and le Roex, 2008). A mantle source for the Dahanib intrusion is confirmed by the Th/Ta versus Ta/Hf diagram (fig. 8B), on which both the mafic and ultramafic samples plot very close to the depleted mantle (DM) compositions of Salters and Stracke (2004) and Workman and Hart (2005) and the primitive upper mantle value of McDonough and Sun (1995), with limited crustal input. The very low concentrations of Nb, Ta, Zr and Hf indicate derivation from a mantle source depleted by a previous melt extraction. This is supported by the data presented by Khedr and Arai (2016). The high-Al spinel and An-rich plagioclase in the ultramafic rocks of the Dahanib intrusion suggest that the magma was originally enriched in both Al and Ca (for example, Dixon, 1981a; Claeson and Meurer, 2004). Furthermore, the rarity of magmatic amphiboles in the ultramafic rocks of Dahanib intrusion argue against a hydrous parental magma and therefore against melting of a source strongly hybridized by fluids derived from a subducted slab (for example, Zhou and others, 2004; Dhuime and others, 2007; Zhao and Zhou, 2007).

We used the chilled margin composition, olivine gabbronorite sample DH44, as an estimate of a possible primitive, olivine-saturated liquid representing an early stage of magmatic differentiation and applied the quantitative solution to the primary magma problem developed originally by Herzberg and O'Hara (2002) and currently implemented in the PRIMELT3 algorithm of Herzberg and Asimow (2015). This model is designed to be applied to liquids or whole-rocks that have only fractionated olivine since being generated by accumulated fractional melting of a peridotite. It tests for and excludes compositions likely to have fractionated clinopyroxene, those derived from pyroxenite-dominated sources, and those strongly contaminated by volatiles in the source. Sample DH44 passes all these tests as long as the Fe^{2+}/Fe_T ratio assumed is less than 0.92. PRIMELT3 then compares the family of possible parental liquids obtained by incrementally adding liquidus olivine to the observed rock to the family of possible primary melts of peridotite. This typically yields a unique solution that has equal melt fractions inferred from FeO-MgO systematics and from a parameterization in normative mineral projection. Applying this calculation to sample DH44, which has 16.33 weight percent MgO, yields solutions with at least 18.2 weight percent MgO in the primary melt, liquidus olivine composition $Fo_{91.4}$, mantle potential temperature >1517 °C, about 12 percent melting leaving a garnet peridotite residue, and at least 7 percent olivine removal at earlier, unsampled stages of evolution. In many regards, this solution resembles that obtained for Icelandic basalts, in terms of potential temperature, liquidus olivine content, and primary magma MgO content, but with evidence of derivation from higher pressure and less fractionation. This result is consistent with a high-temperature, relatively anhydrous mantle melting event below a thick crust, creating a high-MgO tholeiitic parental melt. It does not resemble the magmatic conditions expected in an island arc setting.

The Dahanib Ultramafic Rocks: Residual, Cumulate or Refertilized Peridotites?

Despite the field relations indicating intrusion at upper-crustal levels, it is important to eliminate the hypothesis that the ultramafic Dahanib suite represents a residual mantle sequence. On the face of it, the chemical compositions of the primary minerals (olivine, pyroxene and spinel) could be found both in residual mantle peridotite and in early crystal cumulates from a primitive mantle melt. However, the petrographic studies demonstrate that the Dahanib ultramafic rocks are cumulates, not restites. The olivine and pyroxenes of the Dahanib ultramafic rocks are optically unstrained, without the kink bands that characterize most mantle olivine and pyroxene (Soustelle and others, 2010). This is confirmed by the Fo content of the olivine (<88 mol. %), which is clearly lower than the Fo content of residual mantle olivine (mostly >88 mol%; Bonatti and Michael, 1989; Arai, 1994). Moreover, the lower NiO (< 0.3 wt.%, fig. 5A) and higher MnO (0.16–0.36 wt.%) contents of olivine relative to mantle olivine (for example Takahashi and others, 1987) are not consistent with a restitic mantle origin. The Cr# of spinel and Fo of co-existing olivine in the Dahanib intrusion plot off the olivine-spinel mantle array (OSMA; Arai, 1994) towards low Fo contents (fig. 8C), which implies that they are cumulate rather than mantle derived peridotites and show a fractional crystallization trend. As noted above, although the major phases of the ultramafic sequence are cumulates, the trace element signature indicates a component of trapped intercumulus melt as well.

Although olivine and spinel are the first crystallizing phases, they were closely followed by pyroxenes, which can be used to assess the pressure of formation. The high Mg# of both orthopyroxene (0.80–0.91) and clinopyroxene (0.85–0.91) in the ultramafic rocks suggest that the evolving mantle melt reached saturation with pyroxenes at an early, near-primary stage (for example Tiepolo and others, 2011). The relation between Al_2O_3 and MgO in orthopyroxene and clinopyroxene is controlled by the crystallization pressure of the magma (DeBari and Coleman, 1989). The orthopyroxene and clinopyroxene of the ultramafic rocks plot inside or cluster along the boundary of the deep crustal field (figs. 9A and 9B). They are not consistent with formation as residues followed by transport from mantle pressures.

In summary, several lines of evidence demonstrate that the studied peridotites are crustal-level ultramafic cumulates and do not represent fragments of mantle peridotite.

Fractional Crystallization and Crustal Contamination

Field and petrographic observations suggest crystal accumulation and fractional crystallization each played a role in the evolution of the Dahanib intrusion. In the ultramafic rocks, olivine and Cr-spinel represent the early cumulate phases. The upwards decrease of MgO, Ni, Cr in the intrusion indicate fractionation of olivine and spinel respectively. The olivine abundance and Fo content of olivine decrease systematically from the ultramafic to the mafic rocks. Early crystallization of these Al- and Ca-poor phases leads to increase in Al_2O_3 and CaO in the remaining melt. Fo content of olivine is well-correlated with Mg# of orthopyroxene and clinopyroxene. Pyroxenes from the mafic samples plot along low-pressure progressive fractional crystallization trends in the Al_2O_3 vs Mg# plots (figs. 9A and 9B). Pyroxenes and plagioclase gradually accumulate after olivine and Cr-spinel, giving rise to the formation of pyroxenite, olivine gabbronorite and gabbronorite. Plagioclase has a long crystallization history, being present in all rock varieties from ultramafic rocks through to gabbros.

The role of fractional crystallization is also evident in systematic correlations among whole-rock major oxide concentrations, including the negative correlation of MgO with Al_2O_3 and the positive correlation of Al_2O_3 and CaO, indicating fractionation of olivine and pyroxenes. A decrease in FeOt and Cr_2O_3 with decreasing MgO

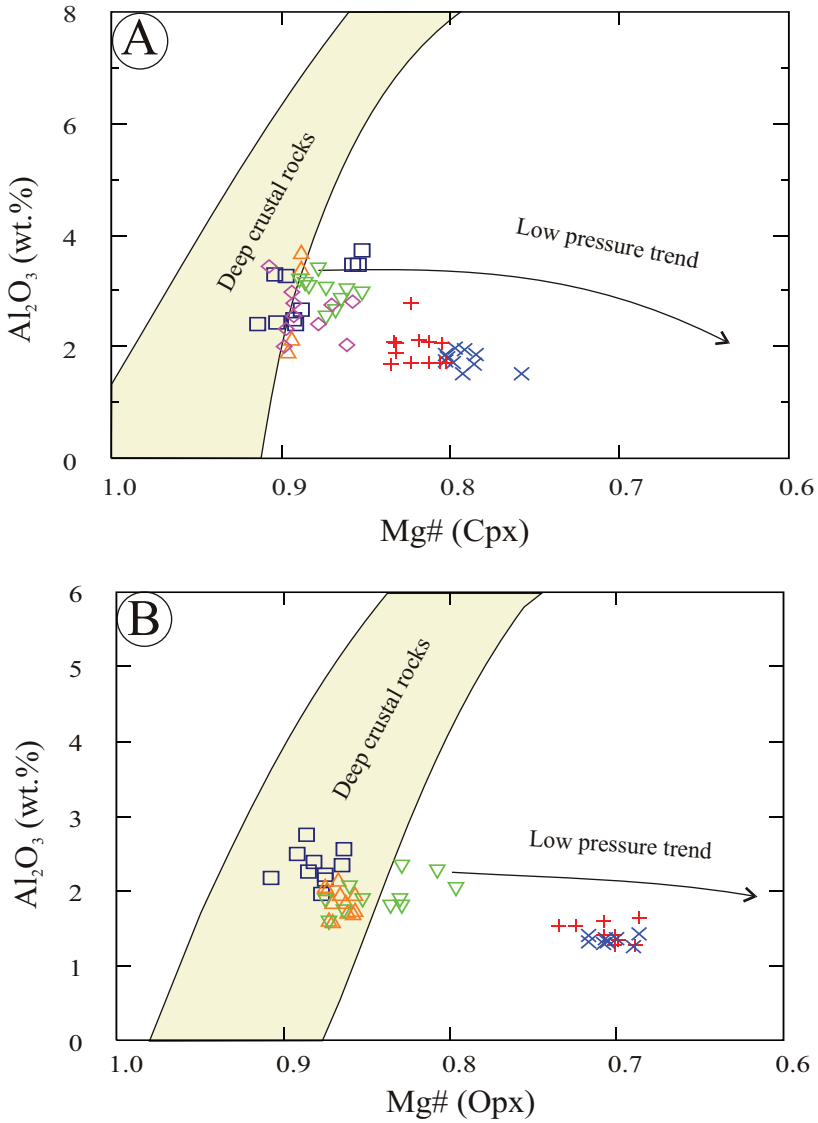

Fig. 9. Al_2O_3 versus Mg# plots for (A) clinopyroxene and (B) orthopyroxene. The pale-yellow field marks deep crustal rocks after DeBari and Coleman (1989). Symbols as in legend of fig. 6A.

indicates chromite fractionation. The trace and REE element patterns of ultramafic and mafic rocks of the Dahanib intrusion have sub-parallel trends indicating the different rock units of the Dahanib intrusion are related to each other by a common parent despite modification by differentiation processes including fractional crystallization.

Fractional crystallization alone, however, cannot explain the gap in most of the major and trace elements between the ultramafic and mafic members. The genetic relationship between the mafic and ultramafic rocks of the Dahanib complex can be considered in a variety of plots (figs. 5 through 9). In most of these views, there is a

substantial gap between the mafic and ultramafic rocks; for example orthopyroxene between Mg# 0.8 and 0.75 and whole-rock HREE concentrations between 3 and 5x chondritic are missing. The presence of such compositional gaps interrupting the fractionation sequence demonstrates that Dahanib is not a fully-exposed and complete differentiation sequence from a single injection of parental magma. Likewise, the absence of gradational contacts between the ultramafic and mafic rocks, the presence of repeated layers in the intrusion (especially the gabbronorites both below and above the pyroxenites), and cross-cutting relationships between gabbroic and ultramafic rocks suggest multiple injections of magma into an open crystallization system. Yet the subparallel trends of the trace element patterns of peridotites and gabbros suggest their derivation by differentiation of similar or identical parental magmas (unless the trace element patterns of the peridotites are dominated by a component of trapped melt similar to the gabbros). A plausible, though non-unique, interpretation of these two sets of observations is that an initial pulse of magma intruded both upper (exposed) and lower (hidden) magma chambers, each of which fractionated to form ultramafic cumulates and residual silicate melts. The upper chamber then received at least one further pulse of buoyant, differentiated magma from the deeper level, which may have mixed with the residual melt and then fractionated to form the exposed mafic members.

We investigated quantitative models of the differentiation sequence using the internally consistent thermodynamic MELTS model of crystal-liquid equilibria (Ghiorso and Sack, 1995), implemented in the alphaMELTS software package (Smith and Asimow, 2005). In particular, we tested whether the chilled margin facies of olivine gabbronorite (sample DH44) could represent a parental liquid from which the ultramafic rocks accumulated, leaving either an evolving liquid line of descent that passes through the mafic rock compositions or subsequent late cumulates that could be represented by the mafic sequence. We considered pressure from 0 to 1 GPa, magmatic oxygen fugacity from 2 log units below to 1 log unit above the quartz-fayalite-magnetite buffer, and initial magmatic water content from 0 to 3 weight percent.

In all cases, MELTS predicts that olivine is the liquidus phase. As the oxygen fugacity increases, the Mg/Fe^{2+} ratio of the melt increases and the liquidus olivine becomes increasingly magnesian, reaching Fo_{91} at QFM+1. Given the maximum Fo content observed in the dunites (0.88), we prefer the reducing end of the explored model space, near QFM-2. As for pressure, above 0.8 GPa the model predicts that garnet appears as a crystallizing phase before plagioclase, which is inconsistent with the observed mineralogy. Furthermore, below 0.2 GPa pressure, plagioclase appears as the second fractionating phase, before clinopyroxene, which is plainly inconsistent with the presence of cumulate wehrlite in the sequence. Hence, we prefer a fractionation pressure in the middle crust, near 0.5 GPa. The results, in terms of phase appearance sequence and coexisting mineral chemistry, are not especially sensitive to the water content in the range explored.

At all pressures considered, the second silicate phase predicted to appear is clinopyroxene when the starting liquid is the whole rock composition of olivine gabbronorite DH-44. This is inconsistent with the presence of a distinct lherzolite layer underlying the wehrlites. Stabilizing near-liquidus orthopyroxene requires higher silica activity in the melt. Hence, we arbitrarily increase the SiO_2 content of the model starting liquid by 4 weight percent. This modified starting liquid, at 0.5 GPa, QFM-2, and 0.5 weight percent H_2O, gives the fractionation sequence olivine (Fo_{89} to Fo_{84}), orthopyroxene (Mg# = 0.88-0.85), clinopyroxene (entering at $Wo_{34}En_{56}Fs_{10}$), Cr-spinel (evolving towards pleonaste), and plagioclase (entering at An_{85} and evolving to An_{55}). This is a reasonable match to both the phase sequence and the coexisting mineral chemistry relations of the ultramafic sequence from dunite through olivine

gabbronorite. Furthermore, fractionation of this assemblage yields a liquid line of descent that produces major and trace element characteristics closely resembling the gabbronorites.

Although this particular model is not unique, and searching the entire model space of plausible primary liquids and fractionation conditions is prohibitive, the robust constraints appear to be sufficient silica activity in the primary liquid to stabilize orthopyroxene as the second crystallizing phase and mid-crustal pressures so as to avoid early garnet or plagioclase. An additional constraint that emerges from the model is the minimum temperature of the initial magma intrusion. The most primitive olivine observed in the dunite, Fo_{88}, would crystallize at 0.5 GPa from the model parental liquid at ~1340 °C with 0.5 weight percent H_2O or at ~1300 °C with 3.0 weight percent H_2O in the melt.

All the mafic rocks in the Dahanib intrusion are characterized by slightly negative Nb-Ta anomalies in the N-MORB normalized trace element diagram (fig. 7B). The depletion of these elements could potentially be explained by crustal contamination, because continental crust is poor in these elements (for example, Rollison 1993). However, extensive crustal contamination would have produced positive Zr-Hf anomalies and high Th/Nb (Land Mclennan, 1995; Yang and Zhou, 2009). Thus, the absence of negative Zr-Hf anomalies and the low Th/Nb (<1) ratios of the Dahanib rocks indicate that crustal contamination was not an important process in the formation of this body. Also, the Dahanib complex contains few xenoliths, except for undigested stoped blocks of upper-level country rock near the chamber roof, arguing against a significant role of crustal contaminations in the evolution of this intrusion. The ratios of Nb/Yb (0.03–0.19) and Th/Yb (0.18–0.67) also do not show evidence for crustal contributions (fig. 8A). The Th/Ta and Ta/Hf ratios of the studied mafic and ultramafic samples are very close to the primitive mantle sources indicating their derivation from partial melting of mantle source without crustal mixing or contamination (fig. 8B). Although the Dahanib samples do show weak enrichment in some HFSE (P, Zr, Hf, Sm) relative to MORB, the overall trace element evidence is most consistent partial melting of a mantle source previously modified by interaction with a fluid-mobilized subduction component, as opposed to high-level contamination by continental crust during transport or emplacement.

The Dahanib Intrusion: Layered Intrusion or Alaskan-Type Intrusion?

As emphasized above, the distinction between Alaskan-type and layered intrusions is important, despite the possibility of confusing them on the basis of geochemical data alone, because Alaskan-type intrusions are specifically associated with island-arc magmatism and imply a tectonic setting of active subduction at the time of their emplacement. The earlier interpretation that the Dahanib intrusion represents a post-orogenic layered intrusion (Dixon, 1981a) was refuted by Khedr and Arai (2016), who concluded to the contrary that it is an Alaskan-type intrusion emplaced during the early subduction-related phase. However, the field evidence presented above supports the clear identification of the Dahanib intrusion as a post-kinematic, undeformed, lopolith-like layered intrusion. It consists of a series of layered cumulate rocks, lacking concentric zoning outwards from an ultramafic core, and quite unlike an Alaskan intrusion.

Khedr and Arai (2016) relied, for their study, on the regional geologic map published by the Geological Survey of Egypt (1992). On this map, the Dahanib intrusion is described as mainly enveloped by gabbronorites and gabbros, a feature cited by Khedr and Arai (2016) as a similarity to other Alaskan-type complexes in the South Eastern Desert. However, we present evidence based on our own field observations that much of the immediate country rock into which the Dahanib body intruded, with well-preserved intrusive contact features exemplified by our field photos, is granodiorite. Also, the concentric zoning described by Khedr and Arai (2016), based

only on the regional geologic map, is crude. In fact, the geometry of the intrusion is roughly circular or elliptical in map-view, and pipe-like in cross-section, with the mafic units on the *inside* of a synformal structure. In order to place the ultramafic rocks in the core of a supposed concentric structure, as in the classic architecture of Alaskan intrusions, Khedr and Arai (2016) consider the syntectonic metamorphic gabbro to the west of the peridotite unit to be part of the Dahanib intrusion and modify the geologic map of Dixon (1981a) to suit. To avoid confusion, this inconsistency in the maps must be studied in the field. We note that the gabbro considered as the outer zone of the Dahanib intrusion by Khedr and Arai (2016) is distinguished by low calcium plagioclase (An_{26-52}, Khedr and Arai, 2016). This is completely different from the plagioclases of the Dahanib intrusion itself (An_{79-94}, Dixon, 1981a; An_{40-82}, the present work) and instead is characteristic of metagabbros in the Eastern Desert of Egypt.

Comparing the Dahanib intrusion with other intrusions in the Eastern Desert of Egypt that are considered to be Alaskan-type (for example Hafez and others, 1991; Helmy and El Mahallawi, 2003; Farahat and Helmy, 2006; Ahmed and others, 2008; Helmy and others, 2008, 2014, 2015; Abd El-Rahman and others, 2012) leads to further objections to the assignment of Dahanib to Alaskan-type by Khedr and Arai (2016). The early subduction phase, the suggested tectonic setting of the Alaskan-type intrusions in Egypt, is represented throughout the Eastern Desert of Egypt by metamorphosed rocks (for example, Bentor, 1985; Abdel-Rahman and Doig, 1987; El-Gabby and others, 1990; Mohamed and Hassanen, 1996; Abu El-Ela, 1997). The Dahanib intrusion is not metamorphosed. Furthermore, the Dahanib intrusion is located along the major NE–SW trending fracture zones that prevail in the South Eastern Desert of Egypt (Garson and Krs, 1976; Farahat and Helmy, 2006; Khedr and Arai, 2016). The emplacement of plutons along these fracture zones is characteristic of the post-orogenic tectonic setting (Garson and Krs, 1976; Moghazi and others, 1999; El-Sayed and others, 2001), not the earlier island arc setting.

In general, most authors agree that distinguishing between Alaskan-type complexes and layered intrusions using geochemistry and mineral chemistry alone is difficult. The reported geochemical and mineral chemistry data for Alaskan-type complexes (for example, Himmelberg and Loney, 1995; Garuti and others, 2002; Ishiwatari and Ichiyama, 2004; Farahat, and Helmy, 2006; Pettigrew and Hattori, 2006; Habtoor and others, 2016) overlap with those reported for layered intrusions (for example Wager and Brown, 1968; Ao and others, 2010; Azer and El-Gharbawy, 2011; Charlier and others, 2015; Abdel Halim and others, 2016). However, in the present work we document a number of mineralogical criteria that distinguish the Dahanib intrusion from an Alaskan-type complex. Clinopyroxene and primary hornblende necessarily occur in all the rock types of the Alaskan-type intrusions (Su, 2013). Orthopyroxene is rare and the gabbro member is only a minor marginal phase in the Alaskan-type intrusions (Helmy and El Mahallawi, 2003; Pettigrew and Hattori, 2006; Su and others, 2012). The Dahanib intrusion does not display any features that are characteristic of typical Alaskan-type bodies: it lacks clinopyroxenite and hornblendite, there is only scarce primary hornblende, and it is notable for abundant orthopyroxene in the ultramafic sequence and plagioclase throughout the mafic layers. Hydrous minerals in Dahanib are rare and represented mainly by secondary amphiboles after pyroxenes in the ultramafic rocks and by minor hornblende in the gabbros. Indeed, the fine-grained gabbro of the chilled margin, the most pristine sample of the mafic magma composition, does not contain any hydrous minerals. These features are all consistent with the characteristics of layered intrusions, although some layered intrusions in the ANS are characterized by an abundance of primary amphiboles (Azer and El-Gharbawy, 2011; Abdel Halim and others, 2016). Green spinel is absent or very rare

in Alaskan-type complexes (Himmelberg and Loney, 1995; Helmy and Mogessie, 2000; Helmy and Mahallawi, 2003; Ahmed and others, 2008; Ben-Xun Su and others, 2012; Ye and others, 2015), but it is common in the Egyptian layered intrusions (Dixon, 1981a; Azer and El-Gharabawy, 2011).

The mineral chemistry data of the Dahanib intrusion are distinct from compositions found in ophiolites and Alaskan-type intrusions, and similar to those of layered intrusions emplaced in stable cratonic settings. The composition of plagioclase in the Dahanib intrusion changes from An_{80} to An_{85} in the lower ultramafic unit and from An_{40} to An_{82} in upper mafic unit, forming cryptic layering similar to, for example, the Bushveld Layered intrusion (Sen, 2014). The low Mg# of olivine (< 0.89) distinguishes the Dahanib intrusion from ophiolitic mafic–ultramafic complexes in the Eastern Desert of Egypt (Azer and Stern, 2007; Khalil and others, 2014; Gahlan and others, 2015; Obeid and others, 2016), except that olivines analyzed from chromitite layers in the Dahanib (Dixon, 1981a; Khedr and Arai, 2016) have high Mg# (0.91-0.94). The Cr-spinel compositions of Dahanib samples, for example on the Mg# versus Fe^{3+}# diagram of Kepezhinskas and others (1993), plot strictly in the field of stratiform layered intrusions rather than in the alpine-type or Alaskan-type fields (fig. 5H).

Comparison with Other Layered Intrusions

Layered intrusions represent intermediate to deep crustal magma chambers that were exposed by tectonic uplift and subsequent erosion of the cap. They are highly variable in their size; the Bushveld intrusion of South Africa (64,000 km^2) is the largest layered intrusion and the Skaergaard intrusion of Greenland (170 km^2) is one of the smallest. Although the Dahanib intrusion is small, its form is similar to the Bushveld Complex; both are inwardly dipping lopoliths of mafic-ultramafic cumulate rocks. The Bushveld Complex shows multiple cycles of both rhythmic and cryptic layering (rhythmic layering is defined by conspicuous variations in abundances of dark and light minerals on a megascopic scale; cryptic layering is defined by chemical compositional change only discernible after determining compositions of the minerals). The Dahanib intrusion expresses only one or two cycles of rhythmic layering, captured by the map-scale lithologic sequence, and of cryptic layering represented by olivine and plagioclase composition changes with height in the intrusion.

Compositional gaps in the crystallization sequence are observed in both the Dahanib intrusion and the Bushveld Complex. The ranges of mineral chemistry are similar as well (Teigler and Eales, 1996; Roelofse and Ashwal, 2012; Yudovskaya and others, 2013). The olivine from the lower ultramafic unit at Dahanib has Fo contents (0.79–0.88, av. 85) nearly similar to the lower zone of the Bushveld Complex (up to 0.85). Although the exposed upper zone of the Bushveld Complex (Fo < 0.50) reaches much more evolved composition than anything seen at Dahanib (Fo 0.79–0.81, av. 79, in the mafic part), the evolution of coexisting olivine, plagioclase and orthopyroxene compositions follow similar trends in the two intrusions.

Comparing the Dahanib intrusion with, by contrast, the Skaergaard intrusion, there are some clear differences. The Skaergaard intrusion remains mafic throughout and is box-shaped (McBirney, 1996; Boudreau and McBirney, 1997; Nielsen, 2003). It was tilted by about 20 degrees southward after it cooled down and crystallized (Schwarz and others, 1979; Farla, 2004). Olivine at the base of the exposed part of the Skaergaard intrusion (Fo = 0.68) is already more evolved than the mafic unit of the Dahanib intrusion, and at Skaergaard the evolution reaches pure fayalite in the sandwich horizon. This is the most important characteristic of the Skaergaard intrusion, whose pronounced trend of iron rather than silica enrichment has made it the type example of a tholeiitic magmas evolution sequence.

Structurally, the Dahanib intrusion has the form of an inwardly dipping lopolith similar to the Abu Fas intrusion, the largest layered intrusion in the South Eastern Desert (Sadek and El-Ramly, 1996). Both intrusions consist of a basal suite of ultramafic rocks and an overlying suite of mafic rocks. Geochemically and mineralogically, the Dahanib intrusion is very similar to tilted layered intrusions in Egypt such as the Imleih mafic-ultramafic intrusion in southern Sinai (Azer and El-Gharbawy, 2011) and the El-Motaghairat intrusion in the South Eastern Desert (Abdel Halim and others, 2016).

CONCLUSIONS

- The Dahanib intrusion is part of the juvenile continental crust of the ANS, exposed in the South Eastern Desert of Egypt. It was emplaced in intermediate to deep crustal level with sharp contacts with the country rocks (metamorphic rocks, granodiorite and gabbro/diorite). It contains scarce stoped blocks of country rocks, and there are numerous offshoots extending from the intrusion into the country rocks. Field observations document that the Dahanib intrusion was emplaced *in situ*, remains remarkably undeformed, and preserves compositional layering with high-angle dip in the lower, ultramafic units and lower-angle dip in the upper, mafic units.
- The ultramafic rocks of the Dahanib intrusion include cumulate dunite, peridotite (lherzolite and wehrlite) and pyroxenite (olivine websterite and websterite). A few thin chromitite layers and nodules are observed within the ultramafic rocks. The contacts between the different ultramafic rocks are sharp. The ultramafic units are sometimes interlayered with gabbro or intruded by it.
- Evidence for multiple injections of magma into the Dahanib complex includes repetition of the mafic units and a substantial gap in both whole-rock and mineral compositions between the most evolved pyroxenite and the least evolved olivine gabbronorite.
- The field studies and mineral chemistry data of the Dahanib intrusion indicate that it is neither an ophiolite fragment or an Alaskan-type intrusive complex, but instead similar in all aspects to layered intrusions emplaced into stable cratonic settings.

ACKNOWLEDGMENTS

We are indebted to Geological Science Department, National Research Centre, Egypt for their support. Special thanks are paid to King Saud University, Deanship of Scientific Research, Research Group No. RG-1436-036 for their support. PDA is supported in part by the US National Science Foundation geoinformatics program, award number EAR-1550934. MKA's Post-doctoral mission to the Division of Geological and Planetary Sciences, California Institute of Technology (Caltech), USA, was supported by the Cairo Initiative of the US Agency for International Development. MKA is indebted to Professor George Rossman and Dr. Michael Baker, California Institute of Technology, for their kind assistance during his post-doctoral mission in Caltech. Special thanks to Dr. Chi Ma for his help with the microprobe analyses.

REFERENCES

Abd El-Rahman, Y., Helmy, H. M., Shibata, T., Yoshikawa, M., Arai, S., and Tamura, A., 2012, Mineral chemistry of the Neoproterozoic Alaskan-type Akarem Intrusion with special emphasis on amphibole: Implications for the pluton origin and evolution of subduction-related magma: Lithos, v. 155, p. 410–425, https://doi.org/10.1016/j.lithos.2012.09.015

Abdel Halim, A. H., Helmy, H. M., Abd El-Rahman, Y. M., Shibata, T., El Mahallawi, M. M., Yoshikawa, M., and Arai, S., 2016, Petrology of the Motaghairat mafic ultramafic complex, Eastern Desert, Egypt: A

high-Mg post-collisional extension-related layered intrusion: Journal of Asian Earth Sciences, v. 116, p. 164–180, https://doi.org/10.1016/j.jseaes.2015.11.015
Abdel-Rahman, A. M., and Doig, R., 1987, The Rb-Sr geochronological evolution of the Ras Gharib segment of the northern Nubian shield: Journal of the Geological Society, London, v. 144, n. 4, p. 577–586, https://doi.org/10.1144/gsjgs.144.4.0577
Abu El-Ela, F. F., 1997, Geochemistry of an island-arc plutonic suite: Wadi Dabr intrusive complex, Eastern Desert, Egypt: Journal of African Earth Science, v. 24, n. 4, p. 473–496, https://doi.org/10.1016/S0899-5362(97)00076-6
Ahmed, A. A., 1991, Ultrabasic and basic intrusions of Um Ginud and Motaghairat area, South Eastern Desert, Egypt: Bulletin Faculty of Science of Assuit University, v. 20, p. 183–213.
Ahmed, A. H., Helmy, H. M., Arai, S., and Yoshikawa, M., 2008, Magmatic unmixing of spinel from late Precambrian concentrically-zoned mafic-ultramafic intrusions, Eastern Desert, Egypt: Lithos, v. 104, n. 1–4, p. 85–98, https://doi.org/10.1016/j.lithos.2007.11.009
Ali, K. A., Azer, M. K., Gahlan, H. A., Wilde, S. A., Samuel, M. D., and Stern, R. J., 2010, Age constraints on the formation and emplacement of Neoproterozoioc ophiolites along the Allaqi-Heiani suture, South Eastern Desert of Egypt: Gondwana Research, v. 18, n. 4, p. 583–595, https://doi.org/10.1016/j.gr.2010.03.002
Ao, S. J., Xiao, W. J., Han, C. M., Mao, Q. G., and Zhang, J. E., 2010, Geochronology and geochemistry of Early Permian mafic–ultramafic complexes in the Beishan area, Xinjiang, NW China: Implications for Late Paleozoic tectonic evolution of the southern Altaids: Gondwana Research, v. 18, n. 2–3, p. 466–478, https://doi.org/10.1016/j.gr.2010.01.004
Arai, S., 1994, Characterization of spinel peridotites by olivine–spinel compositional relationships: Review and interpretation: Chemical Geology, v. 113, n. 3–4, p. 191–204, https://doi.org/10.1016/0009-2541(94)90066-3
Arculus, R. J., and Wills, K. J. A., 1980, The petrology of plutonic blocks and inclusions from the Lesser Antilles Island Arc: Journal of Petrology, v. 21, n. 4, p. 743–799, https://doi.org/10.1093/petrology/21.4.743
Azer, M. K., and El-Gharbawy, R. I., 2011, The Neoproterozoic layered mafic-ultramafic intrusion of Gabal Imleih, south Sinai, Egypt: Implications of post-collisional magmatism in the north Arabian-Nubian Shield: Journal of African Earth Sciences, v. 60, n. 4, p. 253–272, https://doi.org/10.1016/j.jafrearsci.2011.03.010
Azer, M. K., and Stern, R. J., 2007, Neoproterozoic (835–720 Ma) serpentinites in the Eastern Desert, Egypt: Fragments of forearc mantle: The Journal of Geology, v. 115, n. 4, p. 457–472, https://doi.org/10.1086/518052
Azer, M. K., Abu El-Ela, F. F., and Ren, M., 2012, The petrogenesis of late Neoproterozoic mafic dyke-like intrusion in south Sinai, Egypt: Journal of Asian Earth Sciences, v. 54–55, p. 91–109, https://doi.org/10.1016/j.jseaes.2012.04.005
Barrett, T. J., and Maclean, W. H., 1999, Volcanic sequences, lithochemistry and hydrothermal alteration in some bimodal volcanic-associated massive sulfide systems, *in* Barrie, C. T., and Hannington, M. D., editors, Volcanic-associated Massive Sulfide Deposits: Processes and Examples in Modern and Ancient Setting: Reviews in Economic Geology, v. 8, p. 101–131, https://doi.org/10.5382/Rev.08.01
Beard, J. S., 1986, Characteristic mineralogy of arc-related cumulate gabbros: Implications for the tectonic setting of gabbroic plutons and for andesite genesis: Geology, v. 14, n. 10, p. 848–851, https://doi.org/10.1130/0091-7613(1986)14<848:CMOACG>2.0.CO;2
Be'eri-Shlevin, Y., Samuel, M. D., Azer, M. K., Rämö, O. T., Whitehouse, M. J., and Moussa, H. E., 2011, The Ediacaran Ferani and Rutig volcano-sedimentary successions of the northernmost Arabian–Nubian Shield (ANS): New insights from zircon U-Pb geochronology, geochemistry and O-Nd isotope ratios: Precambrian Research, v. 188, n. 1–4, p. 21–44, https://doi.org/10.1016/j.precamres.2011.04.002
Bentor, Y. K., 1985, The crustal evolution of the Arabo-Nubian Massif with special reference to Sinai Peninsula: Precambrian Research, v. 28, n. 1, p. 1–74, https://doi.org/10.1016/0301-9268(85)90074-9
Bilqees, R., Jan, M. Q., Khan, M. A., and Windley, B. F., 2016, Silicate-oxide mineral chemistry of mafic–ultramafic rocks as an indicator of the roots of an island arc: The Chilas Complex, Kohistan (Pakistan): Island Arc, v. 25, n. 1, p. 4–27, https://doi.org/10.1111/iar.12130
Bonatti, E., and Michael, P. J., 1989, Mantle peridotites from continental rifts to oceanic basins to subduction zones: Earth and Planetary Science Letters, v. 91, n. 3–4, p. 297–311, https://doi.org/10.1016/0012-821X(89)90005-8
Bonatti, E., Ottonello, G., and Hamlyn, P. R., 1986, Peridotites from the island of Zabargad (St. John), Red Sea: Petrology and Geochemistry: Journal of Geophysical Research, v. 91, n. B1, p. 599–631, https://doi.org/10.1029/JB091iB01p00599
Bosch, D., and Bruguier, O., 1998, An early Miocene age for a high-temperature event in gneisses from Zabargad Island (Re Sea, Egypt): Mantle diapirism?: Terra Nova, v. 10, n. 5, p. 274–279, https://doi.org/10.1046/j.1365-3121.1998.00202.x
Boudier, F., Nicolas, A., Ji, S., Kienast, J. R., and Mevel, C., 1988, The gneiss of Zabargad Island: Deep crust of a rift: Tectonophysics, v. 150, n. 1–2, p. 209–227, https://doi.org/10.1016/0040-1951(88)90302-2
Boudreau, A. E., and McBirney, A. R., 1997, The Skaergaard Layered Series. Part III. Non-dynamic Layering: Journal of Petrology, v. 38, n. 8, p. 1003–1020, https://doi.org/10.1093/petroj/38.8.1003
Brueckner, H. K., ElHaddad, M. A., Hamelin, B., Hemming, S., Kröner, A., Reisberg, L., and Seyler, M., 1995, A Pan African origin for the gneisses and peridotites of Zabargad Island, Red Sea: A Nd, Sr, Pb, Os isotope study: Journal of Geophysical Research-Solid Earth, v. 100, n. B11, p. 22283–22297, https://doi.org/10.1029/95JB02247
Charlier, B., Namur, O., Latypov, R., and Tegner, C., 2015, Layered Intrusions: Dordrecht, Heidelberg, New York, Springer, 748 p.

Church, W. R., 1983, Precambrian evolution of Afro-Arabian crust from ocean arc to craton: Discussion: Geological Society of America Bulletin, v. 94, n. 5, p. 679–681, https://doi.org/10.1130/0016-7606(1983)94<679:PEOACF>2.0.CO;2
Claeson, D. T., and Meurer, W. P., 2004. Fractional crystallization of hydrous basaltic "arc-type" magmas and the formation of amphibole-bearing gabbroic cumulates: Contributions to Mineralogy and Petrology, v. 147, n. 3, p. 288–304, https://doi.org/10.1007/s00410-003-0536-0
Class, C., and le Roex, A. P., 2008, Ce anomalies in Gough Island lavas -Trace element characteristics of a recycled sediment component: Earth and Planetary Science Letters, v. 265, n. 3–4, p. 475–486, https://doi.org/10.1016/j.epsl.2007.10.030
Cox, K. G., Bell, J. D., and Pankhurst, R. J., 1979, The Interpretation of Igneous Rocks: London, England, Allen & Unwin, 450 p.
DeBari, S. M., and Coleman, R. G., 1989, Examination of the deep levels of an island arc: Evidence from the Tonsina ultramafic–mafic assemblage, Tonsina, Alaska: Journal of Geophysical Research-Solid Earth, v. 94, n. B4, p. 4373–4391, https://doi.org/10.1029/JB094iB04p04373
Dhuime, B., Bosch, D., Bodinier, J. L., Garrido, C. J., Bruguier, O., Hussain, S. S., and Dawood, H., 2007, Multistage evolution of the Jijal ultramafic–mafic complex (Kohistan, N Pakistan): Implications for building the roots of island arcs: Earth and Planetary Science Letters, v. 261, n. 1–2, p. 179–200, https://doi.org/10.1016/j.epsl.2007.06.026
Dick, H. B., and Bullen, T., 1984, Chromian spinel as a petrogenetic indicator in abyssal and Alpine-type peridotites and spatially associated lavas: Contributions to Mineralogy and Petrology, v. 86, n. 1, p. 54–76, https://doi.org/10.1007/BF00373711
Dixon, T. H., 1981a, Gebel Dahanib, Egypt: A late Precambrian layered sill of komatiitic composition: Contributions to Mineralogy and Petrology, v. 76, n. 1, p. 42–52, https://doi.org/10.1007/BF00373682
——— 1981b, Age and chemical characteristics of some pre-Pan-African rocks in the Egyptian Shield: Precambrian Research, v. 14, n. 2, p. 119–133, https://doi.org/10.1016/0301-9268(81)90017-6
El Sharkawy, M. A., and El Bayoumi, R. M., 1979, The ophiolites of Wadi Ghadir area, Eastern Desert, Egypt: Annals of Geological Survey of Egypt, v. 9, p. 125–135.
El-Gaby, S., List, F. K., and Tehrani, R., 1990, The basement complex of the Eastern Desert and Sinai, *in* Said, R., editor, The Geology of Egypt: Rotterdam, Brookfield, Balkema, p. 175–184.
El-Ramly, M. F., 1972, A new geological map for the basement rocks in the Eastern and Southwestern Deserts of Egypt, scale 1:1,000,000: Annals of Geological Survey of Egypt, v. 2, p. 1–18.
El-Sayed, M. M., Furnes, H., Obeid, M. A., and Hassanen, M. A., 2001, The Mueilha intrusion, Eastern Desert, Egypt: A post-orogenic, peraluminous, rare metal bearing granite: Chemie der Erde, v. 61, n. 4, p. 294–316.
Essawy, M. A., El-Metwally, A. A., and Althaus, E., 1997, Pan-African layered mafic-ultramafic-mafic cumulate complex in the SW Sinai massif: Mineralogy, geochemistry and crustal growth: Chemie der Erde, v. 57, p. 137–156.
Farahat, E. S., and Helmy, H. M., 2006, Abu Hamamid Neoproterozoic Alaskan-type complex, south Eastern Desert, Egypt: Journal of African Earth Sciences, v. 45, n. 2, p. 187–197, https://doi.org/10.1016/j.jafrearsci.2006.02.003
Farla, R. J. M., 2004, The Skaergaard Layered Intrusion, East Greenland: The mechanisms of the formation of layering and the trend of differentiation revisited: Report submitted to the Department of Petrology, Utrecht University, 19-11-2004.
Gahlan, H. A., Azer, M. K., and Khalil, A. E. S., 2015, The Neoproterozoic Abu Dahr ophiolite, South Eastern Desert, Egypt: Petrological characteristics and tectonomagmatic evolution: Mineralogy and Petrology, v. 109, n. 5, p. 611–630, https://doi.org/10.1007/s00710-015-0397-z
Garfunkel, Z., 1999, History and paleogeography during the Pan-African orogen to stable platform transition: Reappraisal of the evidence from the Elat area and the northern Arabian–Nubian Shield: Israel Journal of Earth Sciences, v. 48, p. 135–157.
Garson, M. S., and Krs, M., 1976, Geophysical and geological evidence of the relationship of Red Sea transverse tectonics to ancient fractures: Geological Society of America Bulletin, v. 87, n. 2, p. 169–181, https://doi.org/10.1130/0016-7606(1976)87<169:GAGEOT>2.0.CO;2
Garuti, G., Pushkarev, V. E., Zaccarini, F., Cabella, R., and Anikina, E., 2002, Chromite-PGE mineralization in the Uktus Alaskan-Type Complex (Central Urals, Russia): 9th International Platinum Symposium, p. 149–152.
Genna, A., Nehlig, P., Le Goff, E., Gguerrot, C., and Shanti, M., 2002, Proterozoic tectonism of the Arabian Shield: Precambrian Research, v. 117, n. 1–2, p. 21–40, https://doi.org/10.1016/S0301-9268(02)00061-X
Geological Survey of Egypt, 1992, Geological Map of Bernice Quadrangle, South Eastern Desert, Egypt: Scale 1: 250,000.
Ghiorso, M. S., and Sack, R. O., 1995, Chemical mass transfer in magmatic processes IV. A revised and internally consistent thermodynamic model for the interpolation and extrapolation of liquid-solid equilibria in magmatic systems at elevated temperatures and pressures: Contributions to Mineralogy and Petrology, v. 119, n. 2–3, p. 197–212, https://doi.org/10.1007/BF00307281
Gill, R., 2010, Igneous rocks and processes: A practical guide: Chichester, England, Wiley-Blackwell, 428 p.
Grieco, G., and Merlini, A., 2012, Chromite alteration processes within Vourinos ophiolite: International Journal of Earth Sciences, v. 101, n. 6, p. 1523–1533, https://doi.org/10.1007/s00531-011-0693-8
Habtoor, A., Ahmed, A. H., and Harbi, H., 2016, Petrogenesis of the Alaskan-type mafic-ultramafic complex in the Makkah quadrangle, western Arabian Shield, Saudi Arabia: Lithos, v. 263, p. 33–51, https://doi.org/10.1016/j.lithos.2016.08.014
Hafez, A. M., Abdel Kader, Z., and Shalaby, I. M., 1991, Zonedmafic–ultramafic complex in Wadi Abu Hamamid, South Eastern Desert: Annals of the Geological Survey of Egypt, v. 27, p. 53–65.
Helmy, H. M., and Mogessie, A., 2001, Gabbro Akarem, Eastern Desert, Egypt: Cu-Ni-PGE mineralization in a

concentrically zoned mafic-ultramafic complex: Mineralium Deposita, v. 36, n. 1, p. 58–71, https://doi.org/10.1007/s001260050286
Helmy, H. M., and El Mahallawi, M. M., 2003, Gabbro Akarem mafic-ultramafic complex, Eastern Desert, Egypt: A Late Precambrian analogue of Alaskan-type complexes: Mineralogy and Petrology, v. 77, n. 1–2, p. 85–108, https://doi.org/10.1007/s00710-001-0185-9
Helmy, H. M., Yoshikawa, M., Shibata, T., Arai, S., and Tamura, A., 2008, Corona structure from arc mafic–ultramafic cumulates: The role and chemical characteristics of late-magmatic hydrous liquids: Journal of Mineralogical and Petrological Sciences, v. 103, n. 5, p. 333–344, https://doi.org/10.2465/jmps.070906
Helmy, H. M., Abd El-Rahman, Y. M., Yoshikawa, M., Shibata, T., Arai, S., Tamura, A., and Kagami, H., 2014, Petrology and Sm–Nd dating of the Genina Gharbia Alaskan type complex (Egypt): Insights into deep levels of Neoproterozoic island arcs: Lithos, v. 198–199, p. 263–280, https://doi.org/10.1016/j.lithos.2014.03.028
Helmy, H. M., Yoshikawa, M., Shibata, T., Arai, S., and Kagami, H., 2015, Sm–Nd dating and Rb-Sr isotope geochemistry and petrology of Abu Hamamid intrusion, Eastern Desert, Egypt: An Alaskan-type complex in a backarc setting: Precambrian Research, v. 258, p. 234–246, https://doi.org/10.1016/j.precamres.2015.01.002
Herzberg, C., and Asimow, P. D., 2015, PRIMELT3 MEGA.XLSM software for primary magma calculation: Peridotite primary magma MgO contents from the liquidus to the solidus: Geochemistry, Geophysics, Geosystems, v. 16, n. 2, p. 563–578, https://doi.org/10.1002/2014GC005631
Herzberg, C., and O'Hara, M. J., 2002, Plume-associated ultramafic magmas of Phanerozoic age: Journal of Petrology, v. 43, n. 10, p. 1857–1883, https://doi.org/10.1093/petrology/43.10.1857
Himmelberg, G. R., and Loney, R. A., 1995, Characteristics and petrogenesis of Alaskan-type ultramafic–mafic intrusions, southeastern Alaska: U.S. Geological Survey Professional Paper 1564.
Hollings, P., and Wyman, D., 1999, Trace element and Sm-Nd systematics of volcanic and intrusive rocks from the 3 Ga Lumby Lake Greenstone belt, Superior Province: Evidence for Archean plume-arc interaction: Lithos, v. 46, n. 2, p. 189–213, https://doi.org/10.1016/S0024-4937(98)00062-0
Irvine, T., 1974, Petrology of the Duke Island ultramafic complex, southeastern Alaska: Geological Society of America Memoirs, v. 138, p. 1–240, https://doi.org/10.1130/MEM138-p1
Ishiwatari, A., and Ichiyama, Y., 2004, Alaskan-type plutons and ultramafic lavas in Far East Russia, Northeast China and Japan: International Geology Review, v. 46, n. 4, p. 316–331, https://doi.org/10.2747/0020-6814.46.4.316
Jagoutz, O., 2014, Arc crustal differentiation mechanisms: Earth and Planetary Science Letters, v. 396, p. 267–277, https://doi.org/10.1016/j.epsl.2014.03.060
Johan, Z., 2002, Alaskan-type complexes and their platinum-group element mineralization, *in* Cabri, L. J., editor, Geology, geochemistry, mineralogy and mineral beneficiation of platinum group elements: Canadian Institute of Mining, Metallurgy and Petroleum, Special Volume 54, p. 669–719.
Johnson, D. M., Hooper, P. R., and Conrey, R. M., 1999, XRF Analysis of Rocks and Minerals for Major and Trace Elements on a Single Low Dilution Li-tetraborate Fused Bead: Advances in X-ray Analysis, v. 41, p. 843–867.
Johnson, P. R., Andresen, A., Collins, A. S., Fowler, A. R., Fritz, H., Ghebreab, W., Kusky, T., and Stern R. J., 2011, Late Cryogenian-Ediacaran history of the Arabian-Nubian Shield: A review of depositional, plutonic, structural, and tectonic events in the closing stages of the northern East African Orogen: Journal of African Earth Sciences, v. 61, n. 3, p. 167–232, https://doi.org/10.1016/j.jafrearsci.2011.07.003
Kepezhinskas, P. K., Taylor, R. N., and Tanaka, H., 1993, Geochemistry of plutonic spinels from the North Kamachatka Arc: Comparisons with spinels from other tectonic settings: Mineralogical Magazine, v. 57, p. 575–589, https://doi.org/10.1180/minmag.1993.057.389.02
Khalil, A. E. S., and Azer, M. K., 2007, Supra-subduction affinity in the Neoproterozoic serpentinites in the Eastern Desert, Egypt: Evidence from mineral composition: Journal of African Earth Sciences, v. 49, n. 4–5, p. 136–152, https://doi.org/10.1016/j.jafrearsci.2007.08.002
Khalil, A. E. S., Obeid, M. A., and Azer, M. K., 2014, Serpentinized peridotites at the north part of the Wadi Allaqi district (Egypt): Implications for the tectono-magmatic evolution of fore-arc crust: Acta Geologica Sinica, v. 88, n. 5, p. 1421–1436, https://doi.org/10.1111/1755-6724.12309
——— 2015, Late Neoproterozoic post-collisional mafic magmatism in the Arabian–Nubian Shield: A case study from Wadi El-Mahash gabbroic intrusion in southeast Sinai, Egypt: Journal of African Earth Sciences, v. 105, p. 29–46, https://doi.org/10.1016/j.jafrearsci.2015.02.003
Khedr, M. Z., and Arai, S., 2016, Petrology of a Neoproterozoic Alaskan-type complex from the Eastern Desert of Egypt: Implications for mantle heterogeneity: Lithos, v. 263, p. 15–32, https://doi.org/10.1016/j.lithos.2016.07.016
Khudeir, A. A., 1995a, Chromian spinel-silicate chemistry in peridotite and orthopyroxenite relicts from ophiolitic serpentinites, Eastern Desert, Egypt: Bulletin of Faculty of Sciences, Assiut University 24, p. 221–261.
——— 1995b, El-Genina El-Gharbia and El-Genina El-Sharkia ultramafic-mafic intrusions, Eastern Desert, Egypt: Geology, petrology, geochemistry and petrogenesis: Bulletin of Faculty Sciences Assiut University 2-F, 177–219.
Le Bas, M. J., 1962, The role of aluminium in igneous clinopyroxenes with relation to their parentage: American Journal of Science, v. 260, n. 4, p. 267–288, https://doi.org/10.2475/ajs.260.4.267
Leake, B. E., Woolley, A. R., Arps, C. E. S., Birch, W. D., Gilbert, M. C., Grice, J. D., Hawthorne, F. C., Kato, A., Kisch, H. J., Krivovichev, V. G., Linthout, K., Laird, J., Mandarino, J., Maresch, W. V., Nickel, E. H., Rock, N. M. S., Schumacher, J. C., Smith, D. C., Stephenson, N. C. N., Ungaretti, L., Whittaker, E. J. W., and Youzhi, V., 1997, Nomenclature of amphiboles: Report of the Subcommittee on Amphiboles of the

International Mineralogical Association Commission on New Minerals and Mineral Names: Mineralogical Magazine, v. 61, n. 2, p. 295–321.
Leterrier, J., Maury, R. C., Thonon, P., Girard, D., and Marchal, M., 1982, Clinopyroxene composition as a method of identification of the magmatic affinities of paleovolcanic series: Earth and Planetary Science Letters, v. 59, n. 1, p. 139–154, https://doi.org/10.1016/0012-821X(82)90122-4
McBirney, A. R., 1996, The Skaergaard intrusion, *in* Cawthorn, R. G., editor, Layered Intrusions: Developments in Petrology, v. 15, p. 147–180, https://doi.org/10.1016/s0167-2894(96)80007-8
McDonough, W. F., and Sun, S. S., 1995, The composition of the Earth: Chemical Geology, v. 120, n. 2–3, p. 223–253, https://doi.org/10.1016/0009-2541(94)00140-4
Meert, J. G., 2003, A synopsis of events related to the assembly of eastern Gondwana: Tectonophysics, v. 362, n. 1–4, p. 1–40, https://doi.org/10.1016/S0040-1951(02)00629-7
Meguid, A. A. A., and El-Metwally, A. A., 1998, Firstly recorded stratiform chromitities in intrusive layered peridotite, south Eastern Desert Egypt: Egyptian Journal of Geology, v. 42, n. 1, p. 183–205.
Merlini, A., Grieco, G., and Diella, V., 2009, Ferritchromite and chromian-chlorite formation in mélange-hosted Kalkan chromitite (Southern Urals, Russia): American Mineralogist, v. 94, n. 10, p. 1459–1467, https://doi.org/10.2138/am.2009.3082
Miyashiro, A., 1978, Nature of Alkalic volcanic rock series: Contributions to Mineralogy and Petrology, v. 66, n. 1, p. 91–104, https://doi.org/10.1007/BF00376089
Moghazi, A. M., Mohamed, F. H., El-Sayed, M. M., and Kanisawa, S., 1999, Geochemistry and petrogenesis of late Proterozoic plutonic rock suites in the Homrit Waggat and El-Yatima areas, Eastern Egypt: 4th International Conference on Geochemistry (Geochem 8), Alexandria University, Egypt, p. 1–21.
Mohamed, F. H., and Hassanen, M. A., 1996, Geochemical evolution of arc-related mafic plutonism in the Umm Naggat district, Eastern Desert of Egypt: Journal of African Earth Sciences, v. 22, n. 3, p. 269–283, https://doi.org/10.1016/0899-5362(96)00018-8
Morimoto, N., Fabries, J., Ferguson, A. K., Ginzburg, I. V., Ross, M., Seifert, F. A., Zussman, J., Aoki, K.,and Gottardi, G., 1988, Nomenclature of pyroxenes: Mineralogical Magazine, v. 52, p. 535–550, https://doi.org/10.1180/minmag.1988.052.367.15
Neal, C. R., and Taylor, L. A., 1989, A negative Ce anomaly in a peridotite xenolith: Evidence for crustal recycling into the mantle or mantle metasomatism?: Geochimica et Cosmochimica Acta, v. 53, n. 5, p. 1035–1040, https://doi.org/10.1016/0016-7037(89)90208-1
Nielsen, T. F. D., 2003, The Shape and Volume of the Skaergaard Intrusion, Greenland: Implications for Mass Balance and Bulk Composition: Journal of Petrology, v. 45, n. 3, p. 507–530, https://doi.org/10.1093/petrology/egg092
Nisbet, E. G., and Pearce, J. A., 1977, Clinopyroxene composition in mafic lavas from different tectonic settings: Contributions to Mineralogy and Petrology, v. 63, n. 2, p. 149–160, https://doi.org/10.1007/BF00398776
Obeid, M. A., Khalil, A. E. S., and Azer, M. K., 2016, Mineralogy, geochemistry, and geotectonic significance of the Neoproterozoic ophiolite of Wadi Arais area, south Eastern Desert, Egypt: Internal Geological Review, v. 58, n. 6, p. 687–702, https://doi.org/10.1080/00206814.2015.1105727
Pearce, J. A., 1983, Role of the sub-continental lithosphere in magma genesis at active continental margins, *in* Hawkesworth, C. J., and Norry, M. J., editors, Continental Basalts and Mantle Xenoliths: Nantwich, United Kingdom, Shiva Press, p. 230–249.
——— 2008, Geochemical fingerprinting of oceanic basalts with applications to ophiolite classification and the search for Archaean oceanic crust: Lithos, v. 100, n. 1–4, p. 14–48, https://doi.org/10.1016/j.lithos.2007.06.016
Pearce, J. A., and Peate, D. W., 1995, Tectonic implications of the composition of volcanic ARC magmas: Annual Review of Earth and Planetary Sciences, v. 23, p. 251–285, https://doi.org/10.1146/annurev.ea.23.050195.001343
Pearce, J. A., Barker, P. F., Edwards, S. J., Parkinson, I. J., and Leat, P.T., 2000, Geochemistry and tectonic significance of peridotites from the South Sandwich arc-basin system, South Atlantic: Contributions to Mineralogy and Petrology, v. 139, n. 1, p. 36–53, https://doi.org/10.1007/s004100050572
Pettigrew, N. T., and Hattori, K. H., 2006, The Quetico Intrusions of Western Superior Province: Neoarchean examples of Alaskan/Ural-type mafic–ultramafic intrusions: Precambrian Research, v. 149, n. 1–2, p. 21–42, https://doi.org/10.1016/j.precamres.2006.06.004
Rickwood, P. C., 1989, Boundary lines within petrologic diagrams which use oxides of major and minor elements: Lithos, v. 22, n. 4, p. 247–263, https://doi.org/10.1016/0024-4937(89)90028-5
Rietmeijer, F. J. M., 1983, Chemical distinction between igneous and metamorphic orthopyroxenes especially those coexisting with Ca-rich clinopyroxenes: A reevaluation: Mineralogical Magazine, v. 47, p. 143–51, https://doi.org/10.1180/minmag.1983.047.343.04
Ripley, E. M., 2009, Magmatic sulfide mineralization in Alaskan-type complexes, *in* Li, C. S., and Ripley, E. M., editors, New Development in Magmatic Ni-cu and PGE Deposits, 7: Beijing, China, Geological Publishing House, p. 219–228.
Roelofse, F., and Ashwal, L. D., 2012, The lower main zone in the northern limb of the Bushveld Complex—a >1.3 km thick sequence of intruded and variably contaminated crystal mushes: Journal of Petrology, v. 53, n. 7, p. 1449–1476, https://doi.org/10.1093/petrology/egs022
Rollinson, H., 1993, Using Geochemical Data: Evaluation, Presentation, Interpretation: United Kingdom, Longman Group UK Ltd., 352 p.
Rudnick, R. L., and Gao, S., 2003. Composition of the continental crust, *in* Rudnick, R. L, editor, v. 3, The Crust: Elsevier, Treatise on Geochemistry, v. 3, p. 1–64, https://doi.org/10.1016/b0-08-043751-6/03016-4
Sadek, M. F., and El-Ramly, M. F., 1996, Geology, geochemistry and tectonic setting of the layered mafic

ultramafic intrusions in Wadi Abu Fas, Wadi Um Domi area, south Eastern Desert, Egypt: Cairo, Egypt, Proceedings of the Geological Survey, Cennturial Conference, Special Publication, n. 75, p. 689–709.
Salters, V. J. M., and Stracke, A., 2004, Composition of the depleted mantle: Geochemistry, Geophysics, Geosystems, v. 5, n. 5, Q05B07, https://doi.org/10.1029/2003GC000597
Saunders, A. D., Tarney, J., and Weaver, S. D., 1980, Transverse geochemical variations across the Antarctic Peninsula: Implications for the genesis of Cal-alkaline magmas: Earth and Planetary Science Letters, v. 46, n. 3, p. 344–360, https://doi.org/10.1016/0012-821X(80)90050-3
Scandolara, J. E., Ribeiro, P. S. E., Frasca, A. A. S., Fuck, R. A., and Rodrigues, J. B., 2014, Geochemistry and geochronology of mafic rocks from the Vespor suite in the Juruena arc, Roosevelt-Juruena terrain, Brazil: Implications for Proterozoic crustal growth and geodynamic setting of the SW Amazonian craton: Journal of South American Earth Sciences, v. 53, p. 20–49, https://doi.org/10.1016/j.jsames.2014.04.001
Schwarz, E. J., Coleman, L. C., and Cattroll, H. M., 1979, Paleomagnetic results from the Skaergaard intrusion East Greenland: Earth and Planetary Science Letters, v. 42, n. 3, p. 437–443, https://doi.org/10.1016/0012-821X(79)90052-9
Sen, G., 2014, Petrology: Principles and practice: Berlin, Springer, 368 p., https://doi.org/10.1007/978-3-642-38800-2
Shackleton, R. M., 1994, Review of late Proterozoic sutures, ophiolitic mélanges and tectonics of eastern Egypt and north Sudan: Geological Rundschau, v. 83, p. 537–546.
Smith, P. M., and Asimow P. D., 2005. Adiabat_1ph: A new public front-end to the MELTS, pMELTS, and pHMELTS models: Geochemistry, Geophysics, Geosystems, v. 6, n. 2, Q02004, https://doi.org/10.1029/2004GC000816
Soustelle, V., Tommasi, A., Demouchy, S., and Ionov, D. A., 2010, Deformation and fluid-rock interaction in the supra-subduction mantle: Microstructures and water contents in peridotite xenoliths from the Avach Volcano, Kamchatka: Journal of Petrology, v. 51, n. 1–2, p. 363–394, https://doi.org/10.1093/petrology/egp085
Stern, R. J., and Hedge, C. E., 1985, Geochronologic and isotopic constraints on late Precambrian crustal evolution in the Eastern Desert of Egypt: American Journal of Science, v. 285, n. 2, p. 97–127, https://doi.org/10.2475/ajs.285.2.97
Stoeser, D. W., and Frost, C. D., 2006, Nd, Pb, Sr and O isotope characterization of Saudi Arabian Shield terranes: Chemical Geology, v. 226, n. 3–4, p. 163–188, https://doi.org/10.1016/j.chemgeo.2005.09.019
Su, B-X., 2013, Mafic-ultramafic Intrusions in Beishan and Eastern Tianshan at Southern CAOB: Petrogenesis, Mineralization and Tectonic Implication: Springer Theses, Berlin, Germany, Springer-Verlag, 211 p.
Su, B-X., Qin, K-Z., Sakyi, P. A., Malaviarachchi, S. P. K., Liu, P-P., Tang, D-M., Xiao, Q-H., Sun, H., Ma, Y-G., and Mao, Q., 2012, Occurrence of an Alaskan-type complex in the Middle Tianshan Massif, Central Asian Orogenic Belt: Inferences from petrological and mineralogical studies: International Geology Review: v. 54, n. 3, p. 249–269, https://doi.org/10.1080/00206814.2010.543009
Sun, S.-S., and McDonough, W. F., 1989, Chemical and isotopic systematics of oceanic basalts: Implications for mantle composition and processes: Geological Society, London, Special Publications, v. 42, p. 313–345, https://doi.org/10.1144/GSL.SP.1989.042.01.19
Takahashi, E., Uto, K., and Schilling, J. G., 1987, Primary magma compositions and Mg/Fe ratios of their mantle residues along mid-Atlantic ridge 29N to 73N: Okayama, Japan, Okayama University Series, Institute of Studies Earth's Interior, Technical Report A9, p. 1–14.
Taylor, S. R., and McLennan, S. M., 1985, The Continental Crust: Its Composition and Evolution: Oxford, United Kingdom, Blackwell, 312 p.
Teigler, B., and Eales, H. V., 1996, The lower and critical zones of the western limb of the Bushveld Complex as intersected by the Nooitgedacht boreholes: Bulletin of Geological Survey of South Africa, v. 111–112, 126 p.
Thakurta, J., Ripley, E. M., and Li, C. S., 2008, Geochemical constraints on the origin of sulfide mineralization in the Duke Island Complex, southeastern Alaska: Geochemistry, Geophysics, Geosystems, v. 9, n. 7, https://doi.org/10.1029/2008GC001982
Tiepolo, M., Tribuzio, R., and Langone, A., 2011, High-Mg andesite petrogenesis by amphibole crystallization and ultramafic crust assimilation: Evidence from Adamello Hornblendites (Central Alps, Italy): Journal of Petrology, v. 52, n. 5, p. 1011–1045, https://doi.org/10.1093/petrology/egr016
Wager, L. R., and Brown, G. M., 1968, Layered igneous rocks: Edinburgh, Scotland, Oliver and Boyd, 588 p.
Wilson, M., 1994, Igneous Petrogenesis: London, Chapman & Hall, London, 466 p.
Workman, R. K., and Hart, S. R., 2005, Major and trace element composition of the depleted MORB mantle (DMM): Earth and Planetary Science Letters, v. 231, n. 1–2, p. 53–72, https://doi.org/10.1016/j.epsl.2004.12.005
Yang, S.-H., and Zhou, M.-F., 2009, Geochemistry of the ~430-Ma Jingbulake mafic– ultramafic intrusion in Western Xinjiang, NM China: Implications for subduction related magmatism in the South Tianshan orogenic belt: Lithos, v. 113, n. 1–2, p. 259–273, https://doi.org/10.1016/j.lithos.2009.07.005
Ye, X.-T., Zhang, C.-L., Zou, H.-B., Zhou, G., Yao, C.-Y., and Dong, Y.-G., 2015, Devonian Alaskan-type ultramafic-mafic intrusions and silicic igneous rocks along the southern Altai Orogen: Implications on the Phanerozoic continental growth of the Altai Orogen of the Central Asian Orogenic Belt: Journal of Asian Earth Sciences, v. 113, Part 1, p. 75–89, https://doi.org/10.1016/j.jseaes.2014.08.008
Yudovskaya, M. A., Kinnaird, J. A., Sobolev, A. V., Kuzmin, D. V., McDonald, I., and Wilson, A. H., 2013, Petrogenesis of the Lower Zone Olivine-Rich Cumulates Beneath the Platreef and Their Correlation with Recognized Occurrences in the Bushveld Complex: Economic Geology, v. 108, n. 8, p. 1923–1952, https://doi.org/10.2113/econgeo.108.8.1923

Zhao, J. H., and Zhou, M. F., 2007, Geochemistry of Neoproterozoic mafic intrusions in the Panzhihua district (Sichuan Province, SW China): Implications for subduction related metasomatism in the upper mantle: Precambrian Research, v. 152, n. 1–2, p. 27–47, https://doi.org/10.1016/j.precamres.2006.09.002

Zhou, M. F., Lesher, C. M., Yang, Z. X., Li, J. W., and Sun, M., 2004, Geochemistry and petrogenesis of 270 Ma Ni–Cu–(PGE) sulfide bearing mafic intrusions in the Huangshan district, Eastern Xinjiang, Northwest China: Implications for the tectonic evolution of the Central Asian orogenic belt: Chemical Geology, v. 209, n. 3–4, p. 233–257, https://doi.org/10.1016/j.chemgeo.2004.05.005